Scientific Research Publishing

Energy and Power Engineering, 2025, 17(6), 107-133
https://www.scirp.org/journal/epe
ISSN Online: 1947-3818
ISSN Print: 1949-243X

Optimizing Thin-Film Solar Cell Performance: A Comparative Numerical Analysis of GaAsN, GaInAsN and GaInAsNSb-Based Structures Using SCAPS-1D

Zamil Sultan*, Sakib Rahman Chowdhury*, Momotaj Jahan, Abir Reza

Department of Electrical and Electronic Engineering, Hajee Mohammad Danesh Science and Technology University, Dinajpur, Bangladesh
Email: *mdzamilsultan@hstu.ac.bd, *sakib.shaon3825@gmail.com

How to cite this paper: Sultan, Z., Chowdhury, S.R., Jahan, M. and Reza, A. (2025) Optimizing Thin-Film Solar Cell Performance: A Comparative Numerical Analysis of GaAsN, GaInAsN and GaInAsNSb-Based Structures Using SCAPS-1D. *Energy and Power Engineering*, **17**, 107-133.
https://doi.org/10.4236/epe.2025.176006

Received: April 21, 2025
Accepted: June 20, 2025
Published: June 23, 2025

Abstract

This research examines the performances of thin-film solar cells utilizing three dilute nitrides based novel absorber layer's materials GaAsN, GaInAsN, and GaInAsNSb, modeled through SCAPS-1D. Comparative analyses evaluated the effects of absorber layer composition, doping densities, thickness variations, and operating temperature on critical photovoltaic parameters, including short-circuit current density (J_{sc}), open-circuit voltage (V_{oc}), fill factor (FF), efficiency (η), and quantum efficiency (QE). In this study, GaInAsN-based solar cell (Cell 2) demonstrated the highest efficiency (34.7%) and short-circuit current density (46.8 mA/cm^2), while GaAsN (Cell 1) shown reduced performance with J_{sc} and efficiency reaching maxima of 33.8 mA/cm^2 and 30.6%, respectively. These two cell's efficiency is better than that of GaAs-based solar cell reported previously. Thus, it is concluded that dilute nitrides based structure is better for photovoltaic application and further addition of indium atoms (In) into dilute nitrides played a vital role on the crystallographic, electrical and optical properties in GaInAsN for producing better performance. The third cell (Cell 3) based on GaInAsNSb exhibited a peak efficiency of 31.6%; however, it did not achieve the same levels of J_{sc} and efficiency as Cell 2 but Cell 1. It seems that the combined effect of In and Sb atoms in GaInAsNSb mitigates the efficiency. Simulations on the proposed structures revealed that Cell 2 maintained superior performance across a range of absorber thicknesses, doping concentrations, and temperatures, showcasing its robustness and adaptability. Cell 3 exhibited better stability compared to Cell 1, especially under diverse environmental conditions. Furthermore, Cell 2 demonstrated larger quantum efficiency in the visible and near-infrared wave-

lengths, indicating its suitability for high-efficiency photovoltaic applications. This research's findings obtained by simulation would be highly advantageous for further experimental verification in order to advance photonics-based nanotechnology and renewable energy, which would help to reduce greenhouse gas emissions and the world's energy crises simultaneously and sustainably.

Keywords

Thin-Flim Solar Cell, GaAs, GaAsN, GaInAsN, GaInAsNSb, Efficiency, Dilute Nitrides, Quantum Efficiency, Comparative Analysis

1. Introduction

The necessity of energy is growing continuously for technological and industrial development on a global scale but fossil petroleum like coal, natural gas and oil etc. have a limited supply. On the other hand, serious environmental pollution caused by the ongoing increase in the amount of carbon dioxide (CO_2) and other greenhouse gases (GHGs) due to industrialized processes and energy ignition is a stark warning to everyone in the last year [1] [2]. Given these conditions, renewable, green, and clean energy sources have garnered a lot of interest due to their ability to both meet the world's massive energy demands [3]-[5] and diminish the amount of greenhouse gases in the environment sustainably. Solar energy is regarded as one of the most important renewable and sustainable energy sources for photovoltaic applications [6] [7], such as solar cells, because it is both vast internationally and ecologically favourable. However, the primary disadvantages of solar cells over conventional systems are their higher cost [8] and relative efficiency restrictions. It is predicted that the matters will be resolved as technology progresses. It is usual practice to use a reasonably broad band gap for single junction solar cells, because more than 1.7 eV is not conducive [9]. The Shockley-Queisser (S-Q) numerical computations determine that the maximum efficiency limit for a single junction solar cell is 33.7% [10]. One way to overcome the limitations of single junction solar cells was to use multi-junction solar cells [11]. Higher light conversion efficiencies that are beyond the theoretical S-Q limit are made possible by multi-junction solar cell structure; however, the structure has a problem with structural complexity. In terms of cost/watt ratio [12], lightweight design [13], and flexible manufacturing process [14], a thin-film solar cell is a more affordable choice to gradually find new and varied uses [15]. Significant research may be conducted on this device to improve its performance by fine-tuning its structure, structural parameters, and fabrication materials. This is because the fundamental performance metrics of solar cells, such as J-V characteristics, quantum efficiency (QE), open circuit voltage (V_{oc}), short circuit current density (J_{sc}), fill-factor (FF) and efficiency (η), can be accurately controlled by fabrication materials and physical configurations.

Diluted nitrides semiconductors, such as $GaAs_{1-x}N_x$, $GaP_{1-x}N_x$, $Ga_yIn_{1-y}As_{1-x}N_x$, $InP_{1-x}N_x$ and $Ga_yIn_{1-y}As_{1-x-z}N_xSb_z$ belong to group III-V compound semiconductors that are created by incorporating a small percentage of N atoms into the host alloys [16] [17]. The electrical, optical, and crystallographic properties of diluted nitrides are greatly influenced by the compositional constituents' properties and amounts, such as nitrogen's short atomic radius, high electronegativity, and percentage of concentration etc. [18]-[20]. Among various dilute nitrides semiconductors, $GaAs_{1-x}N_x$, $Ga_yIn_{1-y}As_{1-x}N_x$, and $Ga_yIn_{1-y}As_{1-x-z}N_xSb_z$ have emerged as promising candidates due to their exceptional advantageous electrical and optical properties that make them ideal for innovative next-generation optoelectronics, particularly photovoltaic applications [21]. Several studies on dilute nitrides based solar cells have been reported previously where reported efficiency is much lower than the expected value [22]-[24]. Therefore, to achieve better performance from the devices, the $GaAs_{1-x}N_x$, $Ga_yIn_{1-y}As_{1-x}N_x$, and $Ga_yIn_{1-y}As_{1-x-z}N_xSb_z$ have been considered as absorber layer materials in this research. The study also explores the effects of N, In and Sb atoms on the performance parameters of the proposed solar cell structures.

The first substance, $GaAs_{1-x}N_x$, is a ternary compound creating when nitrogen (N) atoms replace a small percentage of group-V element As-atoms in the host GaAs alloy. Most notably, GaAs's band-gap reduction takes place via the conduction band as well as lattice constant is drastically lowered by nitrogen atoms [18]. As a result, it possesses abilities to absorb longer-wavelength photons, outstanding absorption coefficients and charge-transport characteristics, which are crucial for high-efficiency solar cells. In addition, this alloy increased photoluminescence (PL) intensity under laser irradiation [25] which is a proof of its dependability and longer operational life. Because of these superior properties, $GaAs_{1-x}N_x$ has been considered as first absorber layer's material of the proposed thin film solar cell structure in this study. The quaternary $Ga_yIn_{1-y}As_{1-x}N_x$ alloy, the second absorber layer material examined in our study, is created when indium (In) atoms are added into $GaAs_{1-x}N_x$alloy to swap out a small percentage of Ga-atom. Because of its special characteristics, $Ga_yIn_{1-y}As_{1-x}N_x$ has been considered a breakthrough material. The In-atom having a higher atomic radius remarkably stretches the lattice structure and band-gap energy. Thus, its lattice parameter can be adjusted for matching with that of either GaAs or Ge for efficient hetero-junction formation and also the band gap energy can be tuned to a suitable value in the optical range, simultaneously by selecting appropriate nitrogen and indium concentrations in this alloy [26] [27]. The introduction of indium further expands the absorption range of GaAsN into the infrared region, allowing GaInAsN cells to absorb photons with wavelengths up to 1100 nm. Thus, it is considered as a candidate for third sub-cell layer in high efficiency multi-junction (MJ) solar cell [28]-[30] and for an active layer substance in high-characteristics-temperatures long-wavelength laser diodes for optical fiber communications [31]-[35]. The adding of antimony (Sb) atoms into $Ga_yIn_{1-y}As_{1-x}N_x$ makes the alloy $Ga_yIn_{1-y}As_{1-x-z}N_xSb_z$. Sb-

atom plays a vital part in adjusting the band gap by the alignment of the valance band in this alloy [36]-[38]. In fact, the simultaneous incorporation of N and Sb atoms into GaAs or GaInAs modifies both the conduction and valance bands respectively, thereby creates a scope to enhance photon absorption capability. Nevertheless, the insertion of Sb also dramatically boosts the material's crystalline and optical qualities [39]. For example, Sb atoms increase photon absorption up to 1300 nm, thereby $Ga_yIn_{1-y}As_{1-x-z}N_xSb_z$ is considered as a potential candidate for the next generation high efficiency multi-junction solar cell application [40]. So, this alloy has been regarded as third material for the absorber layer in this study. Along with taking absorber layer materials into consideration, some innovative materials have been used for window layer, electron transport layer (ETL) and hole transport layer (HTL) layer. GaAs has been employed as a window layer in this study due to its less susceptibility to overheating, less noise productivity in electrical circuit, long-time stability and fairly priced [41]. The adding of aluminum (Al) ions into GaAs makes AlGaAs alloy which have been used as ETL and HTL in this study because it's special optical and electrical characteristics would appropriate for thin-film structure [42] [43]. It is possible to adjust the material's bandgap by Al-atoms concentration to maximize the cell's capacity to absorb light. In the meantime, AlGaAs can be used as a surface passivation layer to GaAs solar cells to lower complicated losses and interfacial trap states, boosting the cells' efficiency and open-circuit voltage [44] [45].

The suggested structures were simulated first by utilizing these materials as discussed above and then the reliance of thicknesses of absorber and buffer layers, doping density of various layers, defect density and temperature on the solar cell's parameters was examined using SCAPS-1D software. The paper is divided into five sections. Section 1 provides a brief overview of the research that was done for this study. Section 2 will address methods and procedures, including a suggested thin-film solar cell fabrication and modelling strategy. Section 3 displays the analysis of J-V characteristics, V_{oc}, J_{sc}, FF, η and QE for different properties of fabricating materials as well as physical structure of thin-film solar. Section 4 will provide a succinct conclusion to the findings.

2. Methods and Methodology

A schematic representation of the proposed thin-film solar cell structure n^+GaAs/n^-AlGaAs/p-absorber layer/p^+AlGaAs/p^{++}GaAs is shown in **Figure 1**. The uppermost n^+ type GaAs layer and n^- AlGaAs were used as window and ETL respectively. The three novel materials GaAsN, GaInNAs, and GaInNAsSb have been used as absorber layer's materials individually in this proposed structure, titled Cell 1, Cell 2 and Cell 3 respectively. The essential data of $GaAs_{1-x}N_x$ with 1.7% nitrogen concentrations (x = 0.017) [46]; $Ga_yIn_{1-y}As_{1-x}N_x$ with 8% indium and 2.8% nitrogen (y = 0.08 and x = 0.028) [47]; and $Ga_yIn_{1-y}As_{1-x-z}N_xSb_z$ with 9% indium, 2.5% nitrogen, and 5.5% antimony (Sb) (y = 0.09, x = 0.025 and z = 0.055) [48] were used in this simulation. The bottom most highly doped p^- type GaAs

and p^+ AlGaAs have been used as window layer and HTL respectively. A depletion layer develops at the pn-junction, which is created by the n^- type AlGaAs layer and the p^- type absorber layer. The solar cell is exposed to $1000\ mW/cm^2$ of sunlight at an operating temperature of $300\ K$ using the global air mass AM 1.5 G spectrum. For the suggested solar cell structure, the optimal values for the series (R_s) and shunt (R_{sh}) resistances have been taken into account. One of the most well-known and trustworthy computer simulation tools, "Solar Cell Capacitance Simulator's one-dimensional simulation software (SCAPS-1D)," was used to model the suggested structure and examine the performance characteristics. Burgelman *et al.* from the University of Gent's Department of Electronics and Information Systems in Belgium developed the program for thin-film solar cells [49]. Solar cell researchers can use this method to efficiently analyse the device structure [50] [51]. Electrical characterisations and spectrum responses of solar cells can be performed with this very helpful tool. The performance characteristics of the solar cell are estimated by the SCAPS-1D program using numerical solutions of the semiconductor continuity equation and Poisson's equation. For the production of thin-film solar cells, many studies have already confirmed that the real findings and the SCAPS-1D theoretical simulation result are in good agreement.

First of all, we have simulated thin-film solar cells with GaAsN alloys as an absorber layer (Cell 1) and investigate the performance by varying different parameters of the structure. Then, to explore the effects of nitrogen, indium and antimony atoms concentration on the performance parameters, similar measurement was also carried-out for GaInAsN (Cell 2) and GaInAsNSb (Cell 3) alloys. Finally, the obtained results have been compared to get optimum performance. The essential data of materials used for the simulation are shown in **Table 1**.

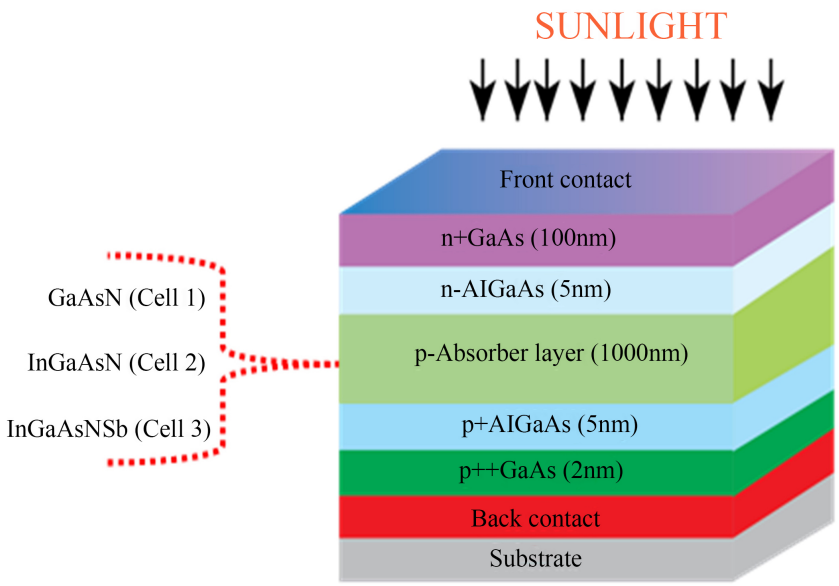

Figure 1. Proposed photovoltaic solar cell (PSC) structure.

Table 1. Essential data of materials used for the SCAPS 1D simulation.

Parameters	$p^{++}GaAs/n^{+}GaAs$ [22]	GaAsN [22] [52] [53]	GaInAsN [54]-[56]	GaInAsNSb [57]	$p^{+}AlGaAs/n^{-}AlGaAs$ [58]-[60]
Thickness (nm)	2/100	1000*	1000*	1000*	5*
Band gap, E_g (eV)	1.42	1.33	1.0	1.0	1.81
Electron affinity, χ (eV)	4.07	4.07	4.0	4.39	3.74
Dielectric permittivity (relative), ϵ_t	12.5	12.38	10.9	12.50	12.10
CB effective density of states, N_c (cm^{-3})	4.33×10^{17}	4.66×10^{17}	1×10^{18}	1×10^{18}	6.25×10^{17}
VB effective density of states, N_v (cm^{-3})	1.28×10^{19}	1.39×10^{19}	1×10^{19}	1×10^{19}	1.12×10^{19}
Electron mobility, μ_n ($cm^2/V-s$)	8.5×10^{3}	6.53×10^{3}	2×10^{3}	5×10^{3}	2.3×10^{3}
Hole mobility, μ_p ($cm^2/V-s$)	4×10^{2}	3.97×10^{2}	2×10^{2}	1.22×10^{2}	1.5×10^{2}
Shallow uniform donor density, N_D (cm^{-3})	$0/1\times10^{16*}$	0	0	0	$0/1\times10^{16*}$
Shallow uniform acceptor density, N_A (cm^{-3})	$1\times10^{16}/0$	$1\times10^{16*}$	1×10^{16}	1×10^{16}	$1\times10^{16*}/0$
Type of defect	Single donor/acceptor	Single donor	Single donor	Single donor	Single donor/acceptor
Defect density, N_t	1×10^{14}	1×10^{14}	1×10^{14}	1×10^{14}	1×10^{14}

Lattice mismatch at the interface between the absorber layer and the window layer were evaluated at the first stage of this study for three absorber layer materials separately because this parameter is a crucial component impacting the structural quality and overall performance of the solar cell. For GaInAsN as an absorber layer material, which includes 8% indium (In) and 2.8% nitrogen (N), the lattice constant is 5.654 Å, resulting in a computed misfit of −0.11% compared to AlGaAs (5.66 Å). This tiny lattice mismatch reflects a very low strain between these two layers, allowing for higher crystal quality and minimum defect development. In the instance of GaInAsNSb, with 9% indium (In), 2.5% nitrogen (N), and 5.5% antimony (Sb), the lattice constant is 5.97 Å, resulting to a more severe positive mismatch of +5.48% with respect to AlGaAs. This bigger mismatch may create strain, which might possibly lead to dislocations but can also enhance material characteristics, such as improved carrier mobility and photon absorption. For GaAsN, with 1.7% nitrogen (N) and a lattice constant of 5.63 Å, the misfit is −0.53% to AlGaAs, showing somewhat higher strain than InGaAsN but still within a reasonable range for retaining acceptable crystal quality. These differences in lattice misfit underline the necessity of exact material composition, notably in the addition of indium, nitrogen, and antimony, to maximize both structural compatibility and higher photovoltaic efficiency.

3. Results and Discussion

According to Figure 1, initially we have simulated the proposed thin-film solar

cell structure with GaAsN alloy as an absorber layer and then investigated the performance through varying different parameters of the structure. Then, to explore the effects of nitrogen, indium and antimony atoms concentration on the performance parameters, similar simulation and measurement were also carried-out individually for two other absorber layer materials GaInAsN and GaInAsNSb. Finally, the obtained results have been compared and analyzed.

3.1. J-V Characteristics of Three Dilute Nitride-Based Photovoltaic Solar Cells—GaAsN, GaInAsN, and GaInAsNSb

First of all, the J-V characteristics of three dilute nitride-based photovoltaic solar cells—GaAsN, GaInAsN, and GaInAsNSb were investigated and then compared as shown in Figure 2 to assess their electrical performance metrics, such as short-circuit current density (J_{sc}), open-circuit voltage (V_{oc}), and overall efficiency (η).

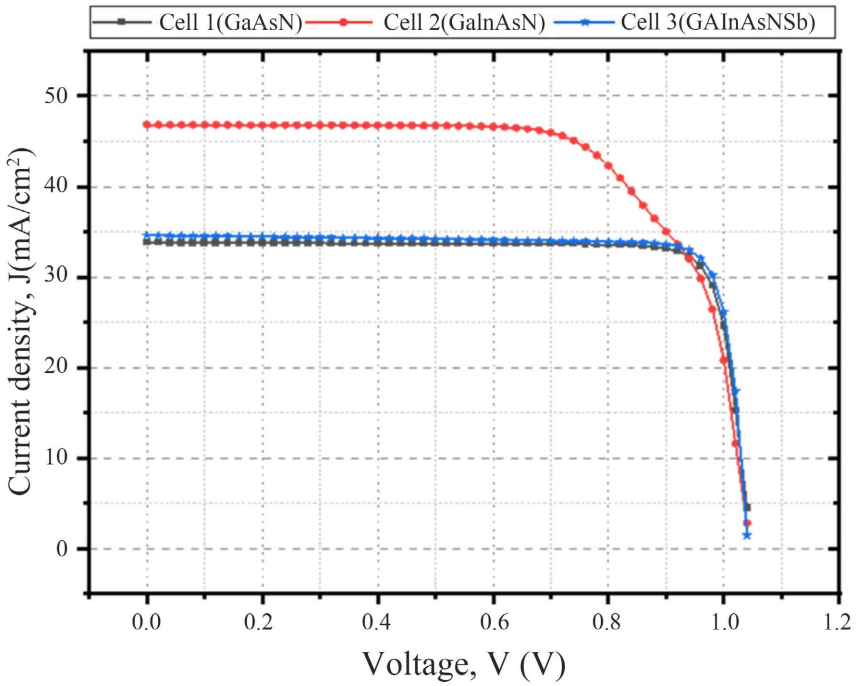

Figure 2. J-V Characteristics of three dilute nitride-based photovoltaic solar cells—GaAsN, GaInAsN, and GaInAsNSb.

As shown in Figure 2, Cell 1 and Cell 3 exhibited nearly similar J-V characteristics while Cell 2 produced comparatively higher short-circuited current density apart from those. It is also noticed that all the three structures produced approximate same open circuited voltage of 1.04 V. It is seen from Figure 2 that GaAsN-based Cell 1 and GaInAsNSb-based Cell 3 produced J_{sc} of ~33.8 mA/cm^2 and of ~34.8 mA/cm^2, respectively while GaInAsN-based Cell 2 produced comparatively higher J_{sc} of ~46.8 mA/cm^2. Thus, the addition of In atoms to GaAsN making GaInAsN is beneficial to be used as absorber layer for improving short circuit current density. Furthermore, the addition of Sb atoms to GaInAsN making

GaInAsNSb is not so effective for improving short circuit current density because it showed a balanced performance comparable to GaAsN. The narrower absorption ranges of GaAsN resulting from its greater band-gap restricted its capacity to collect longer-wavelength photons, leading to a lower J_{sc}. The addition of indium into the GaAsN structure lowered the bandgap, offered lowest lattice mismatch to AlGaAs among the three structures, allowed for improving absorption of near-infrared photons and therefore raised J_{sc}. GaInAsNSb which combines both indium and antimony in GaAsN attained a performance similar to GaAsN. It seems that the combined effect of In and Sb atoms in GaInAsNSb mitigates the effects of each other so that J-V curves of GaAsN-based Cell 1 and GaInAsNSb-based Cell 3 are mostly similar. Antimony's addition to the GaInAsN alloy further stretched the energy bands, optical absorption bands and lattice parameter which may have decreased photon consumption over a wider wavelength range for charge carrier formation and, as a result, decreased the alloy's overall current density in comparison to GaInAsN. Despite the same value of V_{oc} obtained from each cell, the larger value of J_{sc} leads a greater total power output and efficiency, making Cell 2 the most efficient among the three.

3.2. Absorber Layer's Thickness Optimization on Photovoltaic (PV) Parameters

The one of the most crucial factors in improving solar cell performance is the absorber layer's thickness [61]. The investigations shown in **Figures 3(a)-(d)** explore the effects of absorber layer's thickness on the photovoltaic characteristics of the three solar cells, emphasizing differences in J_{sc}, V_{oc}, FF, and η, respectively. It has been noticed that J_{sc} of the three designed cells showed increasing tendency with increasing absorber layer's thickness. However, the value of that parameter for Cell 2 remains relatively in the higher range than other two cells over the whole range of thickness. Cell 1 (GaAsN) displays a continuous increase in J_{sc} from 31.9 to 34.6 mA/cm^2 as thickness climbs to 2.5 μm shown in **Figure 3(a)**, but its V_{oc} stays approximately constant at 1.04 V observed in **Figure 3(b)**, however FF decreases slightly from 87.3% to 85.4% as illustrated in **Figure 3(c)**. Its efficiency peaks at 30.6% at 1.5 μm but saturates subsequently shown in **Figure 3(d)**. Cell 2 (GaInAsN) obtains the maximum performance, with J_{sc} growing from 44.5 to 48.0 mA/cm^2, attributable to improved photon absorption by GaInAsN, while V_{oc} begins at 1.05 V but declines slightly to 1.01 V due to higher recombination in thicker layers. Its FF, ranging from 68.7% to 71.2%, is lower than Cell 1 and Cell 2. However, Cell 2's efficiency achieves a high of 34.7% at 2.5 μm, powered by GaInAsN's adjustable band-gap and greater light absorption. Cell 3 (GaInAsNSb) shows J_{sc} rising from 33.3 to 35.3 mA/cm^2, with V_{oc} stabilizing at 1.04 V and FF maintaining high values (86.2% - 86.3%). Efficiency stabilizes about 31.6%, modestly surpassing Cell 1 but falling short of Cell 2. The research reveals that the GaInAsN structure gives the highest performance because to its greater J_{sc} and efficiency, while the inclusion of antimony in GaInAsNSb increases stability over

the whole range of thickness. From this analysis, we suggested fabricating the proposed thin-film solar cell structure with absorber layer's thickness 1 μm (1000 nm) for obtaining better performances.

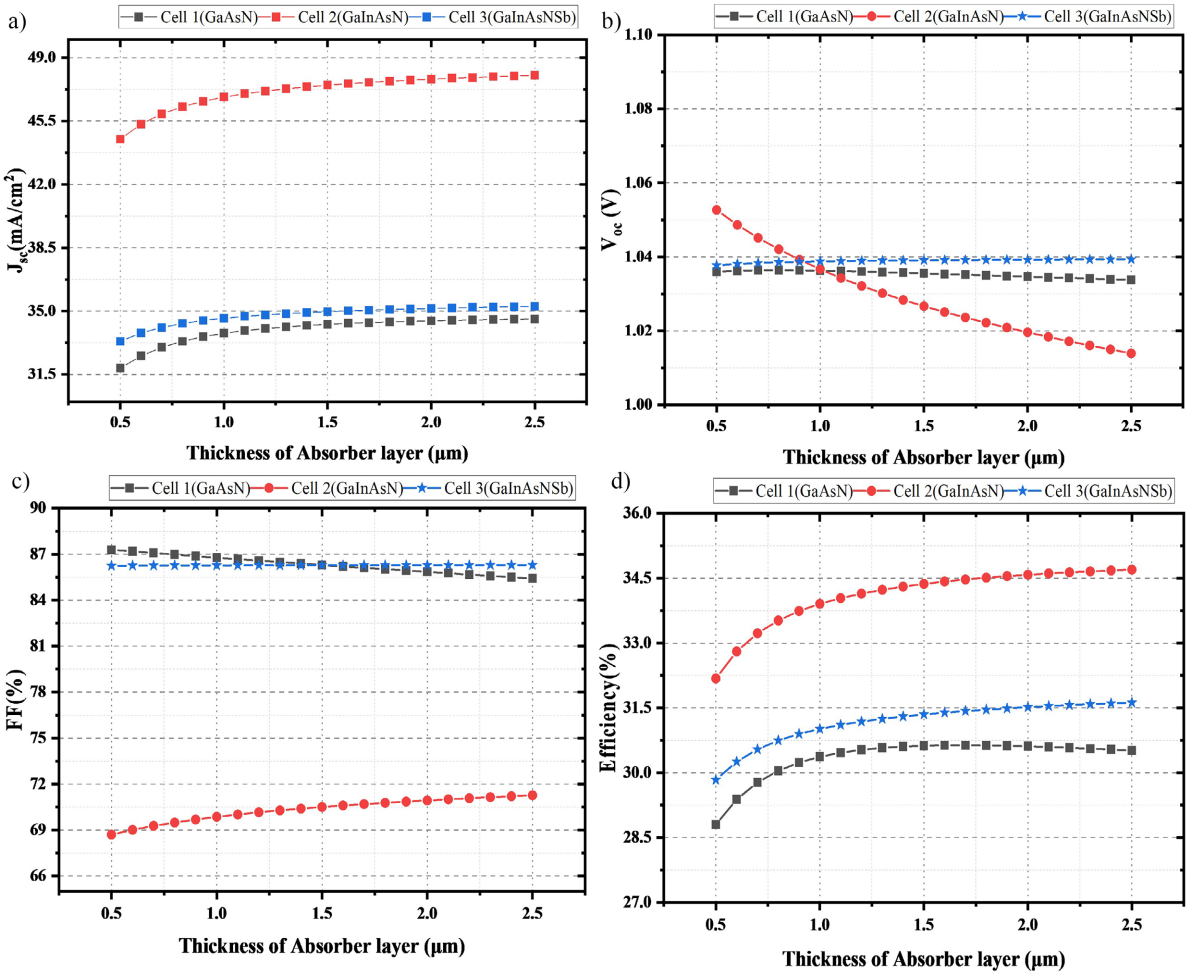

Figure 3. Impact of absorber layer thickness on (a) J_{sc} (b) V_{oc} (c) FF (d) Efficiency, η of Photovoltaic (PV) solar cells.

3.3. Impact of Thickness of Bottom-Most p^{++} GaAs Window Layer on Solar Cell Performance

The section analyzes how increasing the thickness of bottom-most p^{++} GaAs window layer impacts the performance metrics of GaAsN, GaInAsN, and GaInAsNSb-based solar cells, concentrating on J_{sc}, V_{oc}, FF, and efficiency as shown in **Figures 4(a)-(d)** respectively. For the p^{++} GaAs layer, variations in thickness demonstrate negligible influence on overall performance for all three cells. Cell 1 displays about constant J_{sc} values at 33.8 mA/cm^2 in **Figure 4(a)** regardless of thickness, demonstrating that differences in the p^{++} GaAs layer do not substantially impair carrier collection. Similarly, Cell 2 maintains a consistent J_{sc} of 46.8 mA/cm^2 across all thicknesses, suggesting no impact of the layer's thickness on the GaInAsN structure. For Cell 3, J_{sc} marginally rises from 34.6 mA/cm^2 at 2 nm to 35.5 mA/cm^2 at 10 nm before stabilizing, indicating a small enhancement in carrier collection owing to Sb-

enhanced passivation in the GaInAsNSb structure. It has been seen from Figure 4(b) that V_{oc} stays consistent at 1.04 V across all thicknesses for the three cells, showing that modifying the p^{++} GaAs layer thickness does not affect the built-in potential or carrier separation. The FF also stays constant: 86.8% for Cell 1, 69.9% for Cell 2, and 86.3% for Cell 3 as depicted in Figure 4(c), suggesting negligible influence of the p^{++} GaAs layer thickness on the diode properties. Efficiency shown in Figure 4(d) follows a similar trend: it continues at 30.4% for Cell 1 and 33.9% for Cell 2, while Cell 3 shows a tiny rise from 31.0% at 2 nm to 31.9% at 10 nm. This illustrates the p^{++} GaAs layer's principal function as a passivation layer, with negligible impact on carrier transmission or collection. The findings from this section reveal that although the three proposed structures produce similar behavior in all parameters with increasing thickness, but GaInAsN-based structure gives the highest performances. Thus, we proposed the thickness of bottom-most p^{++} GaAs layer should be minimum as possible around 0.002 μm (2 nm).

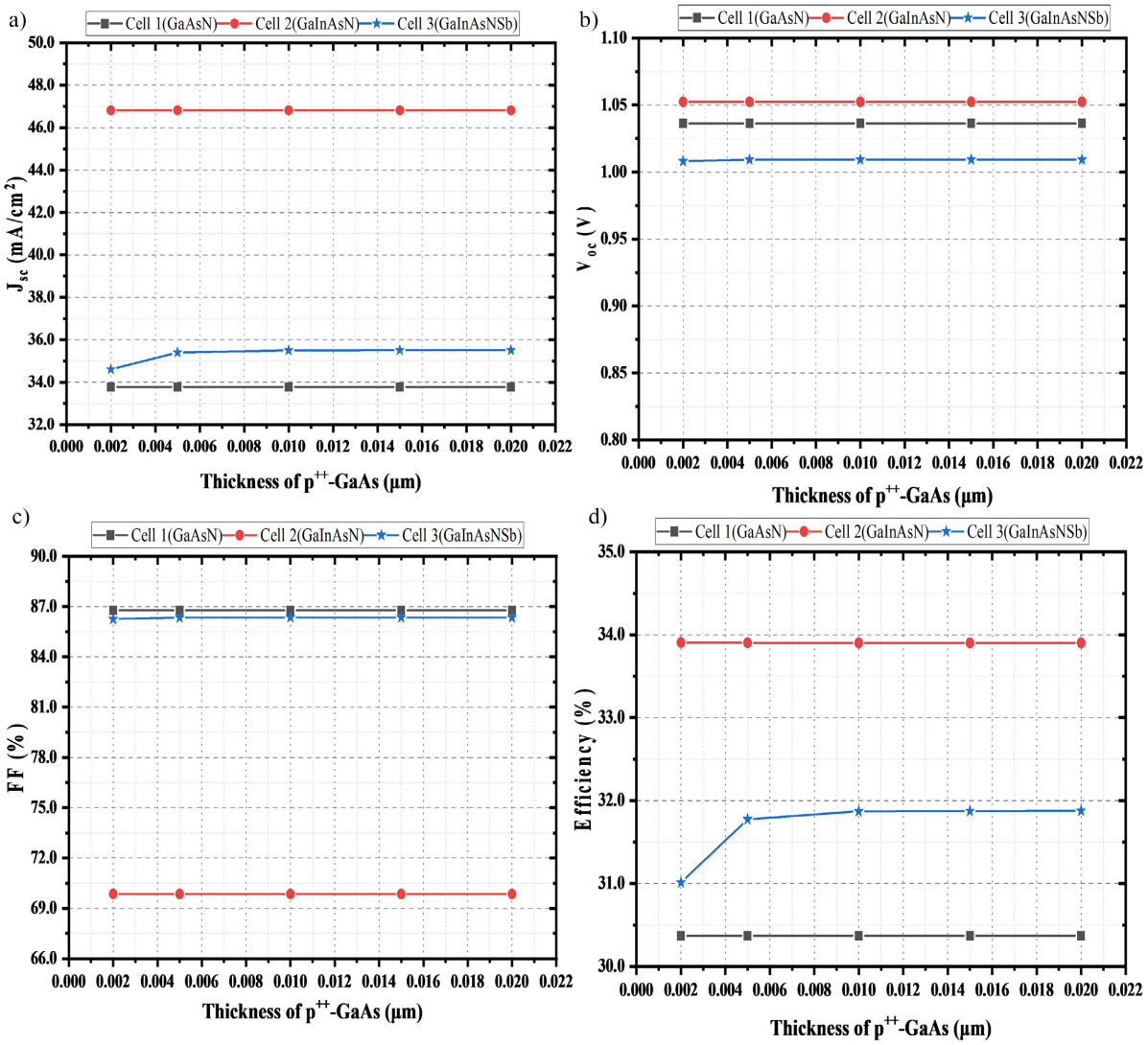

Figure 4. Variation of p^{++} GaAs thickness on (a) J_{sc} (b) V_{oc} (c) FF (d) Efficiency, η on Photovoltaic (PV) solar cells.

3.4. Impact of Thickness of Upper-Most n⁺ GaAs Window Layer on Solar Cell Performance

In contrast to p^{++} GaAs layer, difference in the upper-most n^+ GaAs layer thickness considerably impacts J_{sc} and efficiency, notably for Cells 1 and 2 as demonstrated in Figure 5. For Cell 1, J_{sc} declines drastically from 33.8 mA/cm² at 0.1 μm to 18.5 mA/cm² at 1.5 μm, showing greater recombination losses and lower carrier collecting efficiency in thicker layers. Similarly, Cell 2's J_{sc} drops from 46.8 mA/cm² at 0.1 μm to 31.4 mA/cm² at 1.5 μm.

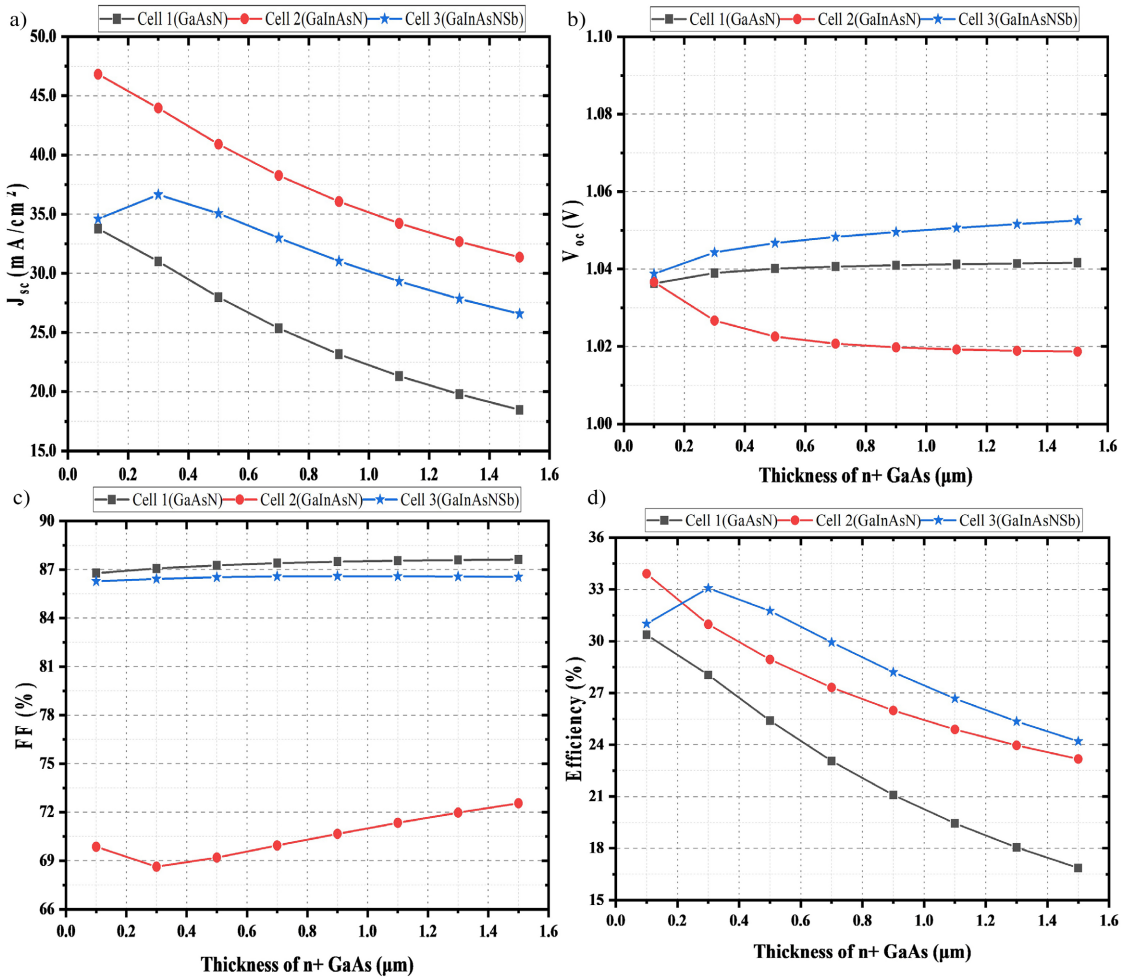

Figure 5. Variation of n^+ GaAs thickness (a) J_{sc} (b) V_{oc} (c) FF (d) Efficiency, η on Photovoltaic (PV) solar cells.

As seen from the Figure 5(a), Cell 3 demonstrates a minor initial rise in J_{sc} from 34.6 mA/cm² at 0.1 μm to 36.6 mA/cm² at 0.3 μm before falling to 26.6 mA/cm² at 1.5 μm, indicating excellent carrier transport at intermediate thicknesses and a reduced influence of recombination losses owing to Sb inclusion. V_{oc} stays steady at 1.04 V throughout all thicknesses for Cell 1, but Cell 2 suffers a little decline from 1.04 V to 1.02 V with increasing thickness. Cell 3 exhibits steady V_{oc} values (1.04 V to 1.05 V), further showing Sb's stabilizing impact as illustrated in Figure 5(b). The FF for Cell 1 rises minimally from 86.8% at 0.1 μm to 87.6% at 1.5 μm,

demonstrating moderate sensitivity to n^+ GaAs layer thickness. Conversely, Cell 2 exhibits a reduction in FF from 69.9% to 68.9% with increasing thickness, whereas Cell 3 maintains a consistent FF of 86.5% shown in Figure 5(c), indicating Sb's involvement in regulating electrical characteristics. In Figure 5(d), efficiency patterns parallel those of J_{sc}: Cell 1's efficiency lowers dramatically from 30.4% at 0.1 μm to 16.9% at 1.5 μm, while Cell 2's dips from 33.9% to 23.2%, owing to increasing recombination losses. For Cell 3, efficiency declines more gradually from 31.0% at 0.1 μm to 24.2% at 1.5 μm, illustrating the durability of the GaInAsNSb structure against thickness fluctuations. Considering J_{sc}, V_{oc} and η, GaInAsN-based structure has been found comparatively better than other two structure. A thickness of around 0.01 μm (100 nm) is advised in this section for the uppermost n^+ GaAs layer for getting improved performance.

3.5. Impact of Thickness of p^+ AlGaAs HTL on Solar Cells Performance

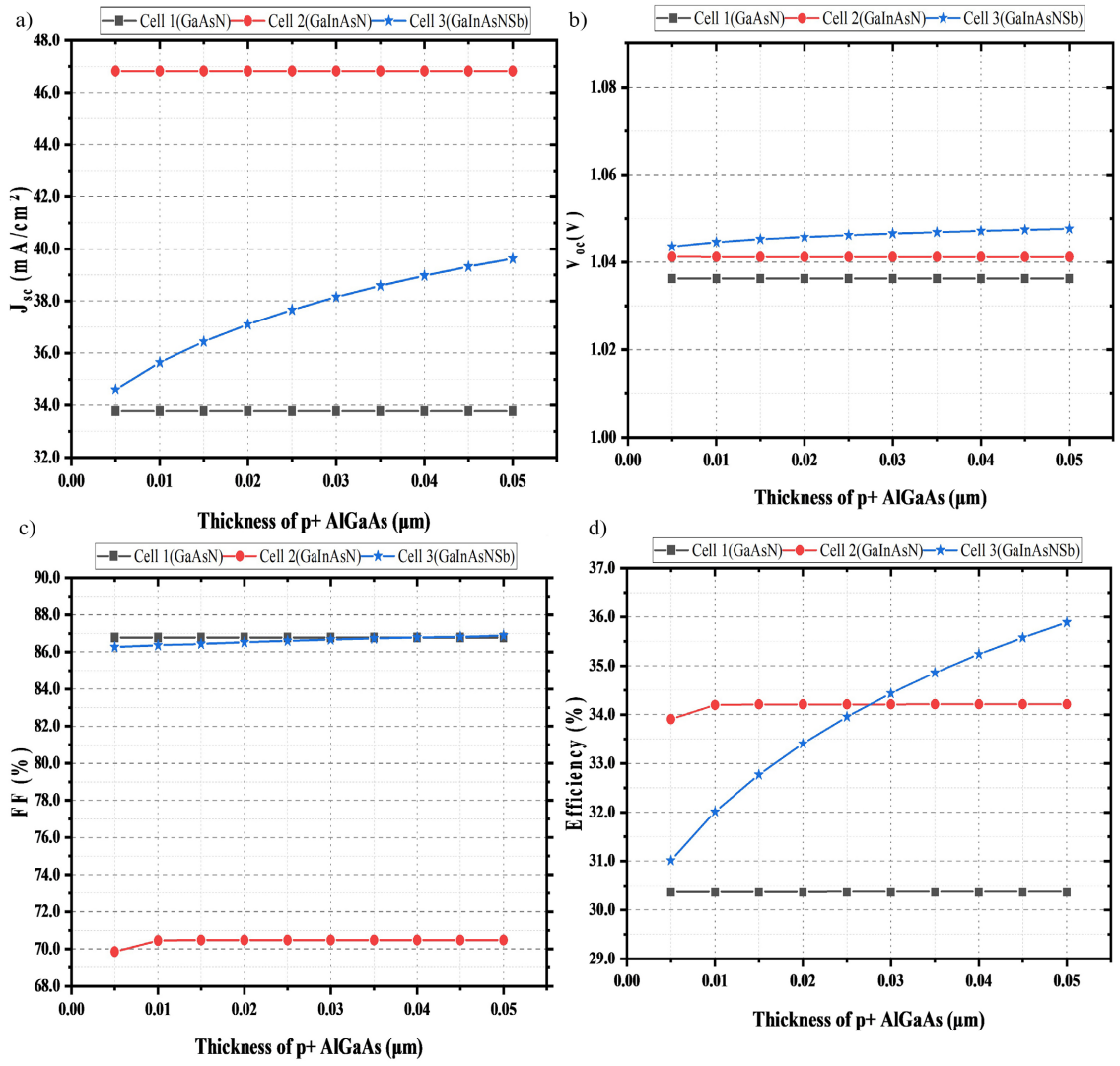

Figure 6. Impact of p^+ AlGaAs HTL thickness on (a) J_{sc} (b) V_{oc} (c) FF (d) Efficiency, η on Photovoltaic (PV) solar cells.

For the p^+ AlGaAs HTL, the findings showed minor influence on Cells 1 and 2, but Cell 3 benefitted from increased thickness of HTL as illustrated in **Figures 6(a)-(d)**.

As demonstrated in **Figure 6(a)**, Cell 1 retains a consistent J_{sc} of 33.8 mA/cm^2 throughout all thicknesses from 5 nm to 50 nm, suggesting that carrier collecting efficiency is unaltered. Cell 2 exhibits a modest drop in J_{sc} from 46.8 mA/cm^2 at thinner layers to 46.5 mA/cm^2 at 50 nm, demonstrating minor effect of the p^+ AlGaAs layer thickness on GaInAsN cells. For Cell 3, however, J_{sc} rises dramatically from 34.6 mA/cm^2 at 5 nm to 39.6 mA/cm^2 at 50 nm, indicating improved carrier collection owing to Sb inclusion. V_{oc} stays fixed at 1.04 V for all three cells over the full thickness range observed in **Figure 6(b)**, demonstrating that the p^+ AlGaAs layer thickness has no influence on the built-in potential or carrier separation. Similarly, FF shown in **Figure 6(c)** remained stable: 86.8% for Cell 1, 69.9% to 70.5% for Cell 2, and 86.3% for Cell 3, exhibiting negligible susceptibility to thickness fluctuations. Efficiency visualized in **Figure 6(d)** also stays consistent for Cells 1 and 2, at 30.4% and 33.9%, respectively, while Cell 3 demonstrates a considerable increase from 31.0% at 5 nm to 35.9% at 50 nm, showing Sb's capacity to boost carrier collection and minimize recombination losses.

3.6. Impact of Thickness of n^- AlGaAs ETL on Solar Cell Performance

Finally, increasing the n^- AlGaAs ETL thickness significantly influences Cells 1 and 2 but has negligible effect on Cell 3 as shown in **Figures 7(a)-(d)**, respectively.

For Cell 1, J_{sc} stays steady at 33.8 mA/cm^2 for thin layers (5 - 10 nm) but declines slightly to 33.5 mA/cm^2 at 50 nm, suggesting minimal recombination or resistance losses. Similarly, Cell 2's J_{sc} declines somewhat from 46.8 mA/cm^2 at thinner layers to 46.5 mA/cm^2 at 50 nm, but Cell 3's J_{sc} stays consistent at roughly 34.6 mA/cm^2 across all thicknesses, showing Sb's function in preserving electron mobility and carrier collection. V_{oc} stays stable at 1.04 V for all three cells, suggesting that n^- AlGaAs layer thickness does not alter the voltage characteristics. The FF for Cell 1 reduces considerably from 86.8% at 5 nm to 66.5% at 50 nm, implying higher series resistance with thicker layers. Cell 2's FF reduces considerably from 73.6% to 68.9%, but Cell 3 maintains a steady FF of 86.3%, further illustrating Sb's stabilizing impact. Efficiency follows similar trends: Cell 1's efficiency reduces drastically from 30.4% at 5 nm to 23.1% at 50 nm, while Cell 2's dips from 33.9% to 33.2%, driven by losses in J_{sc} and FF. In comparison, Cell 3 demonstrates a small drop in efficiency from 31.0% to 30.3%, showing its robustness to thickness fluctuations due to Sb inclusion. Overall, the findings reinforce the crucial significance of thickness optimization in minimizing recombination losses and boosting carrier transport for Cells 1 and 2, whereas Cell 3's performance stability across changing thicknesses shows the benefits of Sb inclusion in the GaInAsNSb structure.

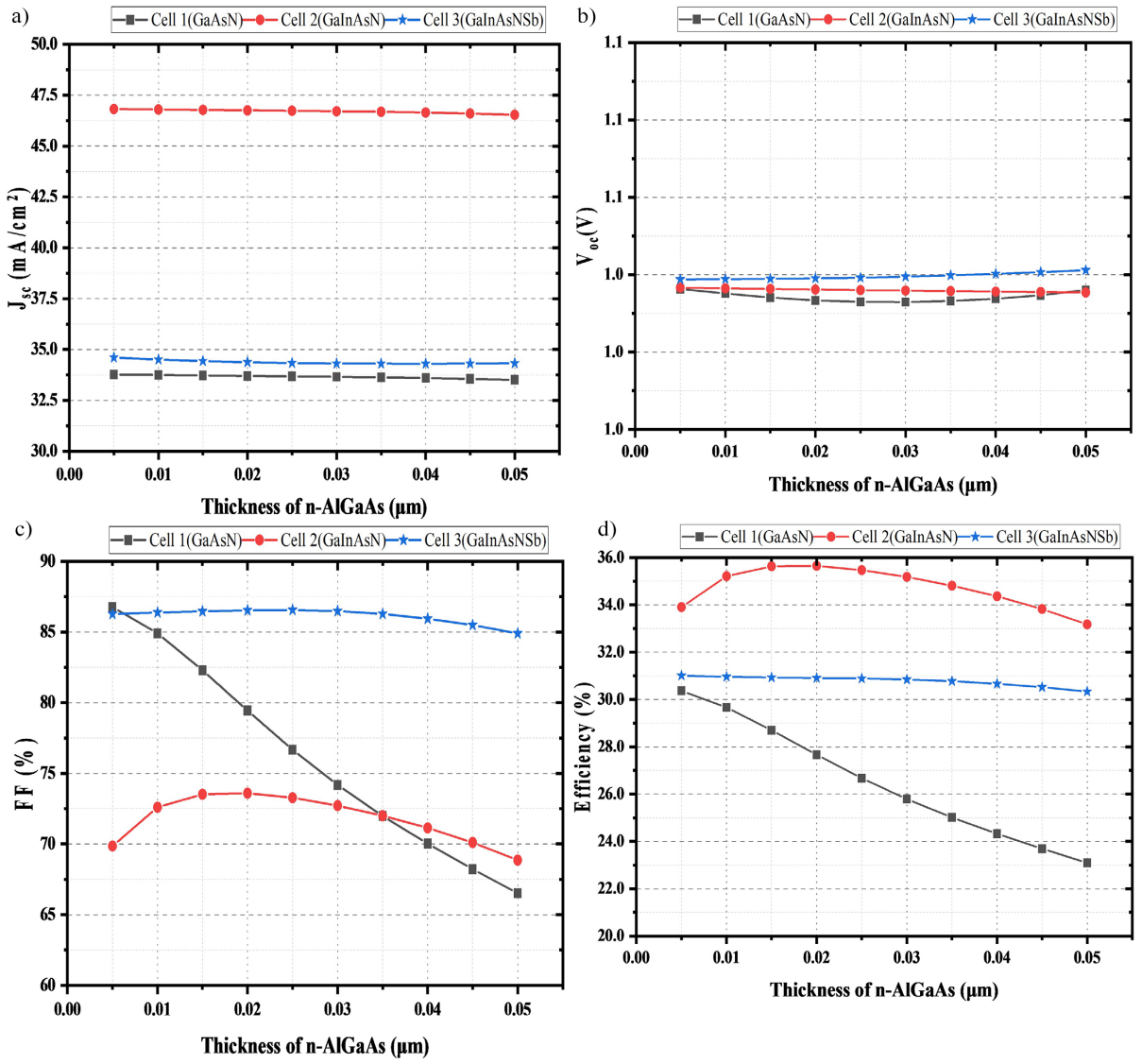

Figure 7. Variation of n⁻ AlGaAs thickness on (a) J_{sc} (b) V_{oc} (c) FF (d) Efficiency, η on Photovoltaic (PV) solar cells.

3.7. Effect of P-Type Absorber Layer's Acceptor Doping Density on PV Parameters

The performance metrics like J_{sc}, V_{oc}, FF, and η of the three solar cell models in Figure 1 are greatly impacted by acceptor density, as indicated in Figures 8(a)-(d), respectively.

For Cell 1, J_{sc} shown in Figure 8(a) initially rises from 32.1 mA/cm^2 at 1×10^{15}cm^{-3} to 33.8 mA/cm^2 at 1×10^{18} cm^{-3} but drops dramatically at higher densities owing to recombination, reaching 22.6 mA/cm^2 at 1×10^{20} cm^{-3}. V_{oc} follows a similar tendency, peaking at 1.04 V with moderate doping before significantly declining as seen from Figure 8(b). FF increases to 86.8% at 1×10^{18} cm^{-3} but plummets to 68.5% at high doping levels, with efficiency peaking at 30.4% before decreasing to 17.9%. For Cell 2, J_{sc} demonstrates a substantial spike from 33.2 mA/cm^2 to 46.8 mA/cm^2 at 1×10^{18} cm^{-3}, due to GaInAsN's higher

absorption capabilities, while V_{oc} grows gradually from 0.916 V to 1.09 V, suggesting effective carrier separation. FF peaks at 76.0% at 1×10^{19} cm^{-3}, with efficiency reaching an amazing 38.7%. Cell 3, adding Sb, maintains consistency across all measures, with J_{sc} and V_{oc} being steady at 34.6 mA/cm^2 and 1.04 V, respectively, and FF at 86.3%, resulting in stable efficiency around 31%. These trends demonstrate that Cell 2 excels in efficiency (38.7%) owing to improved band-gaps and absorption, whereas Cell 3 provides higher stability under variable doping concentrations. Cell 1, while effective at modest doping levels, experiences large losses at greater densities owing to recombination. This research underlines the trade-offs between performance optimization and stability among the cells. Our proposed solar panel's absorber layer should have an acceptor doping density of 1×10^{16} cm^{-3}.

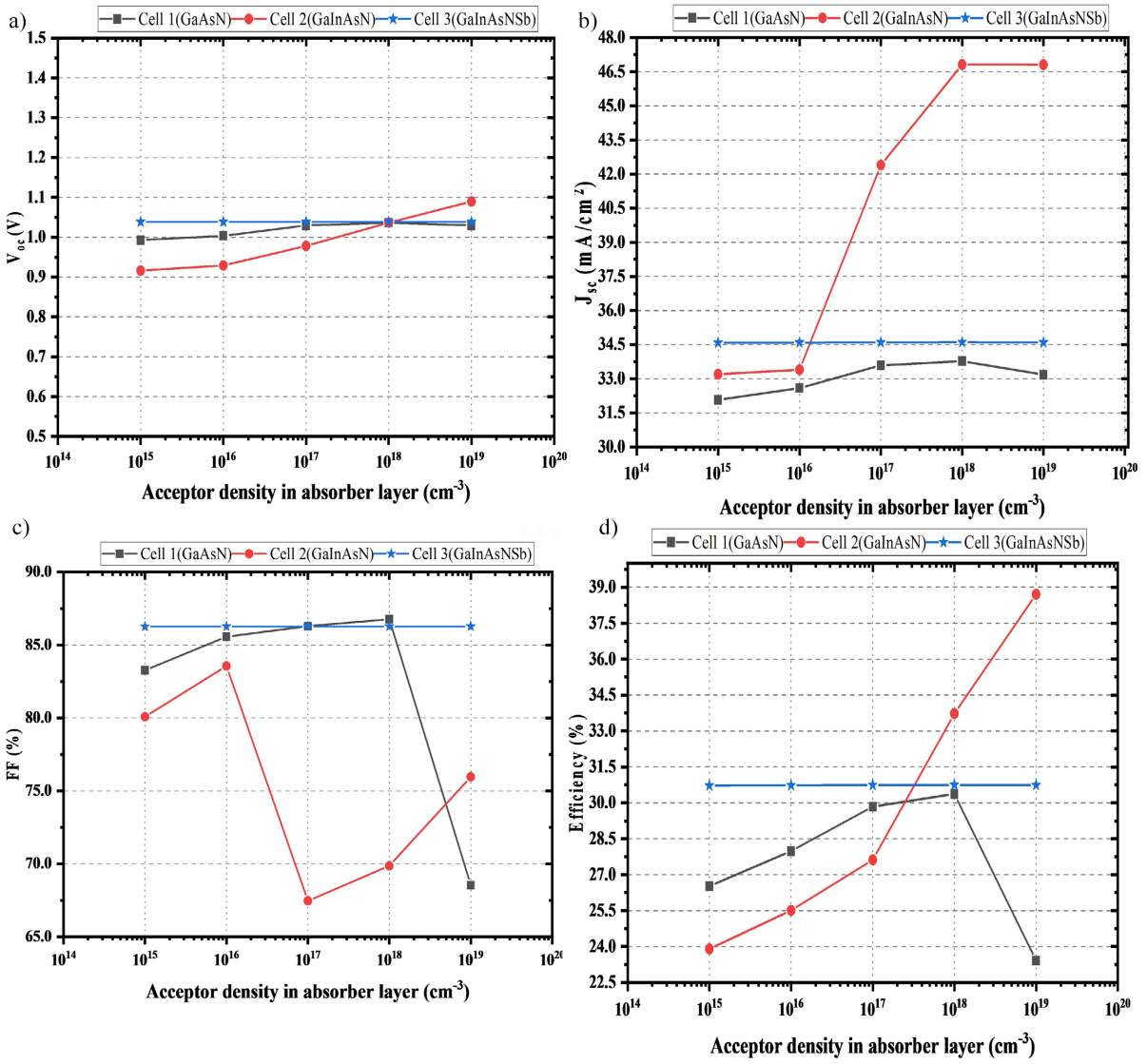

Figure 8. Variation of absorber layer acceptor density on (a) J_{sc} (b) V_{oc} (c) FF (d) Efficiency, η on Photovoltaic (PV) solar cells.

3.8. Influence of n+ GaAs Layer's Donor Doping Density on PV Parameters

The performance of the proposed solar cells is greatly impacted by differences in doping concentrations in various layers, notably the n^+ GaAs, p^+ AlGaAs, and n^- AlGaAs layers. In all designed three cell types, the donor density of the n^+ GaAs layer has a considerable influence on the cell's photovoltaic (PV) properties, including J_{sc}, V_{oc}, FF, and η as illustrated in Figures 9(a)-(d), respectively.

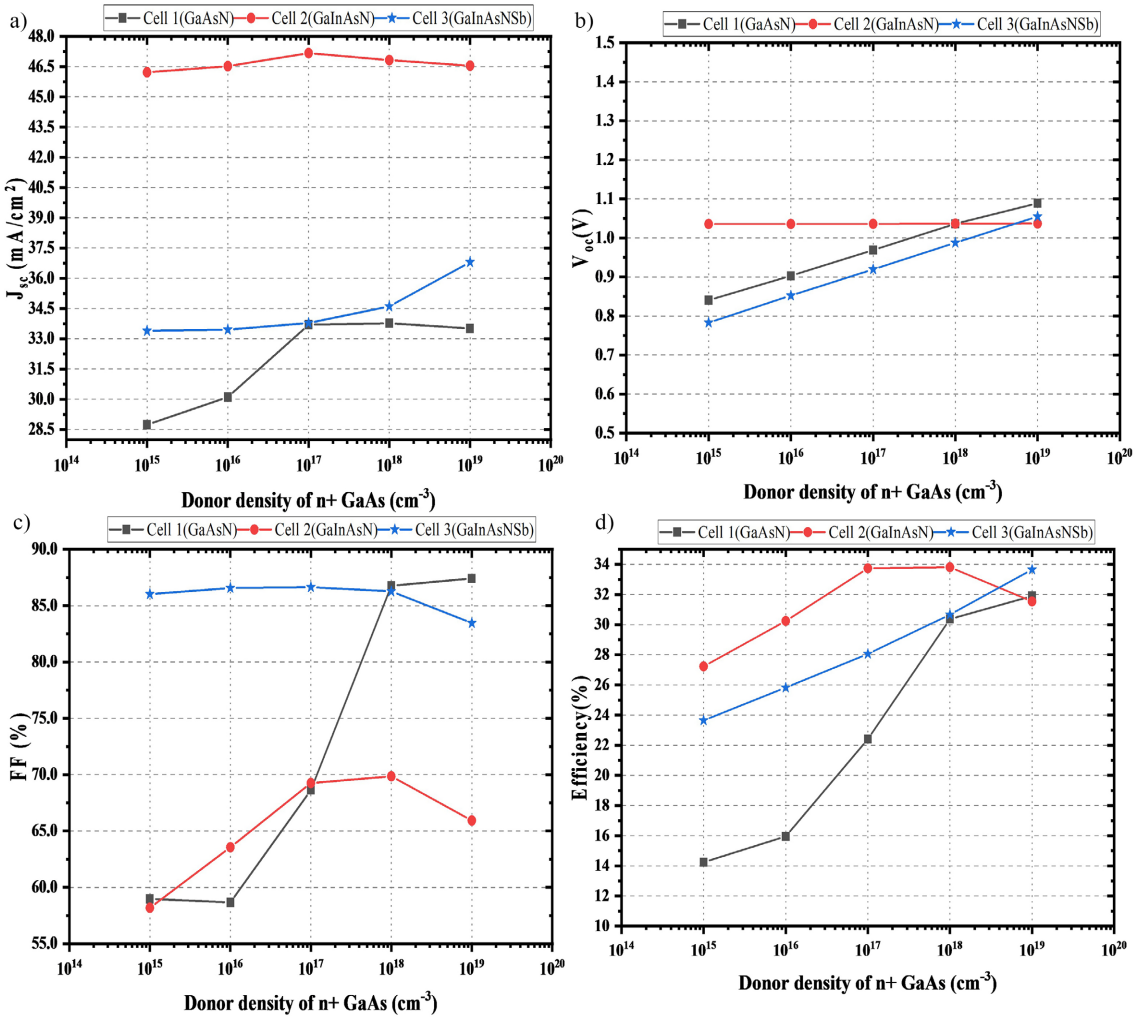

Figure 9. Variation of n^+ GaAs donor density on (a) J_{sc} (b) V_{oc} (c) FF (d) Efficiency, η on Photovoltaic (PV) solar cells.

For Cell 1, increasing the donor density of the n^+ GaAs layer leads in a constant increase in J_{sc}, from 28.7 mA/cm^2 at 1×10^{15} cm^{-3} to 33.5 mA/cm^2 at 1×10^{19} cm^{-3} as seen from Figure 9(a). This is followed by a considerable improvement in V_{oc} of Figure 9(b), which jumps from 0.84 V to 1.09 V, suggesting improved band alignment and less recombination losses. The fill factor shown in Figure 9(c) also rises from 59% to 87.4%, adding to a boost in efficiency from 14.2% to 31.9% as illustrated in Figure 9(d). This improvement is possibly due to the decreased series resistance and better carrier transport associated with increased doping den-

sities. In Cell 2, the J_{sc} rises from 46.2 mA/cm^2 at 1×10^{15} cm^{-3} to 47.2 mA/cm^2 at 1×10^{17} cm^{-3}, but reduces at higher doping levels because to increased recombination, revealing a balance between greater carrier collection and recombination. V_{oc} stays steady at 1.04 V throughout doping densities, whereas FF grows from 58.2% to 69.9%, culminating at moderate doping levels, with efficiency rising from 27.8% to 33.9%. In Cell 3, the J_{sc} climbs gradually from 33.4 mA/cm^2 at low doping densities to 36.8 mA/cm^2 at 1×10^{19} cm^{-3}, boosted by the addition of Sb, which helps retain favorable electron transport and minimize recombination. The V_{oc} rises from 0.855 V to 1.10 V, while FF stays consistent at 86%, suggesting that Sb stabilizes the electrical properties. Efficiency climbs from 24.6% to 33.8%, illustrating the value of Sb in sustaining high performance over a wide range of doping concentrations. The higher values of J_{sc} and efficiency making Cell 2 the most efficient among the proposed three structures. For improved performance, doping the n^+ GaAs layer with an impurity density of 1×10^{17} cm^{-3} is advised.

3.9. Influence of p$^+$ AlGaAs HTL's Acceptor Doping Density on PV Parameters

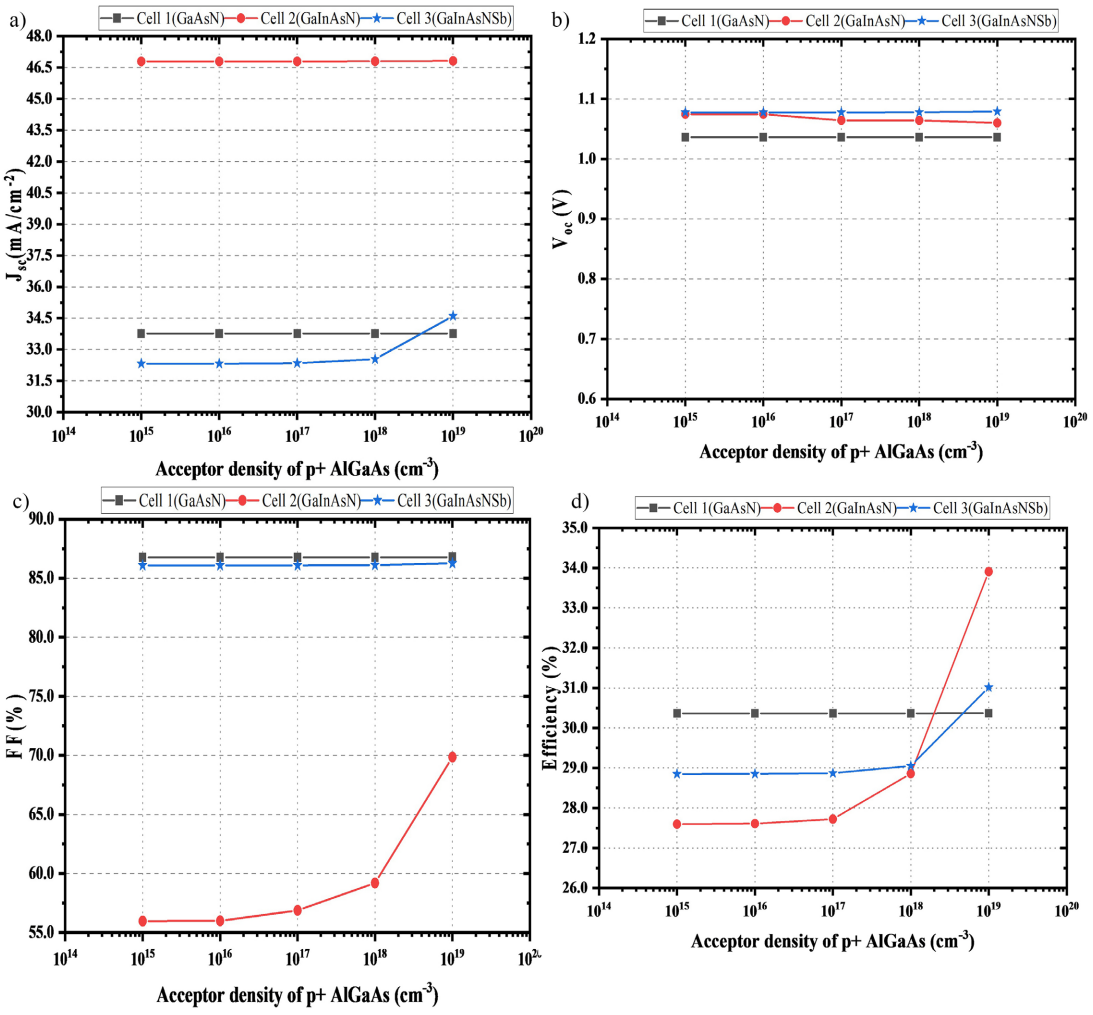

Figure 10. Impact of p$^+$ AlGaAs density on (a) $J_{sc,}$ (b) V_{oc} (c) FF and (d) Efficiency, η on Photovoltaic (PV) solar cells.

Regarding the p^+ AlGaAs layer shown in Figure 10, Cell 1 displays minor changes in J_{sc}, V_{oc}, and efficiency with varied doping densities, demonstrating that p^+ AlGaAs doping does not substantially alter the cell's performance. Similarly, Cell 2 demonstrates consistent performance at lower doping levels, with a modest reduction in V_{oc} at high doping densities, whereas FF improves from 56.0% to 69.9% as doping density grows, leading to a steady efficiency gain from 27.6% to 33.9%. In Cell 3, efficiency climbs slightly from 28.9% to 31.0% as doping increases, demonstrating that the p^+ AlGaAs doping impacts efficiency but with declining returns compared to the n^+ GaAs layer.

3.10. Influence of n^- AlGaAs ETL's Donor Doping Density on PV Parameters

The doping density in the n^- AlGaAs ETL layer has a more substantial influence on the performance of the solar cells as illustrated in Figure 11. For Cell 1, the J_{sc} remains approximately constant at 34.5 mA/cm^2 up to doping density level 1×10^{18} cm^{-3} but declines rapidly at 1×10^{19} cm^{-3} as seen from Figure 11(a) for GaAsN. Similarly, for adding In-atoms, Cell 2 exhibits comparatively higher J_{sc} which declines from 46.8 mA/cm^2 to 33.3 mA/cm^2 after decreasing the doping density from 1×10^{18} cm^{-3} to 1×10^{19} cm^{-3}, attributable to lower electron mobility at higher doping levels. In contrast, Cell 3 displays a rise in J_{sc} from lower doping densities to 36.4 mA/cm^2 at 1×10^{19} cm^{-3}, helped by Sb, which helps maintain excellent carrier transport despite higher doping. It is observed from Figure 11(b) that V_{oc} for Cell 1 climbs from 1.04 V to 1.08 V at high doping densities, showing enhanced carrier separation, whereas Cell 2 and Cell 3 exhibit steady V_{oc} throughout doping densities, proving their tolerance to changes in donor density. The FF shown in Figure 11(c) for Cell 1 reduces rapidly from 87.5% to 71.2% at high doping levels, whereas Cell 2 and Cell 3 also see a fall in FF, albeit less so in Cell 3, where Sb helps preserve stability. The behavior of the FF is possibly dependent on the combined behavior of V_{oc} and J_{sc} [62] [63]. As demonstrated in Figure 11(d), efficiency in Cell 1 declines from 30.6% to 20.5% at large donor densities, reflecting the reduced J_{sc} and FF. Cell 2's efficiency reduces from 34.2% to 29.8%, whereas Cell 3's efficiency climbs somewhat, reaching 32.6% at 1×10^{19} cm^{-3}. The value of η reflects the total behavior of V_{oc}, J_{sc} and FF. The presence of Sb in Cell 3 mitigates the deleterious impacts of higher donor density, resulting to more consistent and better performance across all doping levels. Overall, the findings emphasize that while doping density in the n^+ GaAs and n^- AlGaAs layers significantly influences the efficiency and stability of the solar cells, the incorporation of Sb in the GaInAsN-based cells offers superior performance, particularly in maintaining stable electrical characteristics and achieving high efficiency at a wide range of doping densities. This suggests that careful optimization of doping densities, particularly in the n^+ GaAs and n^- AlGaAs layers is critical for maximizing the performance of GaAsN and GaInAsN-based solar cells. It is also clarified that Sb plays a crucial role in improving their stability and efficiency across varying doping conditions. For n^- AlGaAs ETL, we suggested maintaining a donor doping density level

of 1×10^{16} cm^{-3} in order to get improved performance.

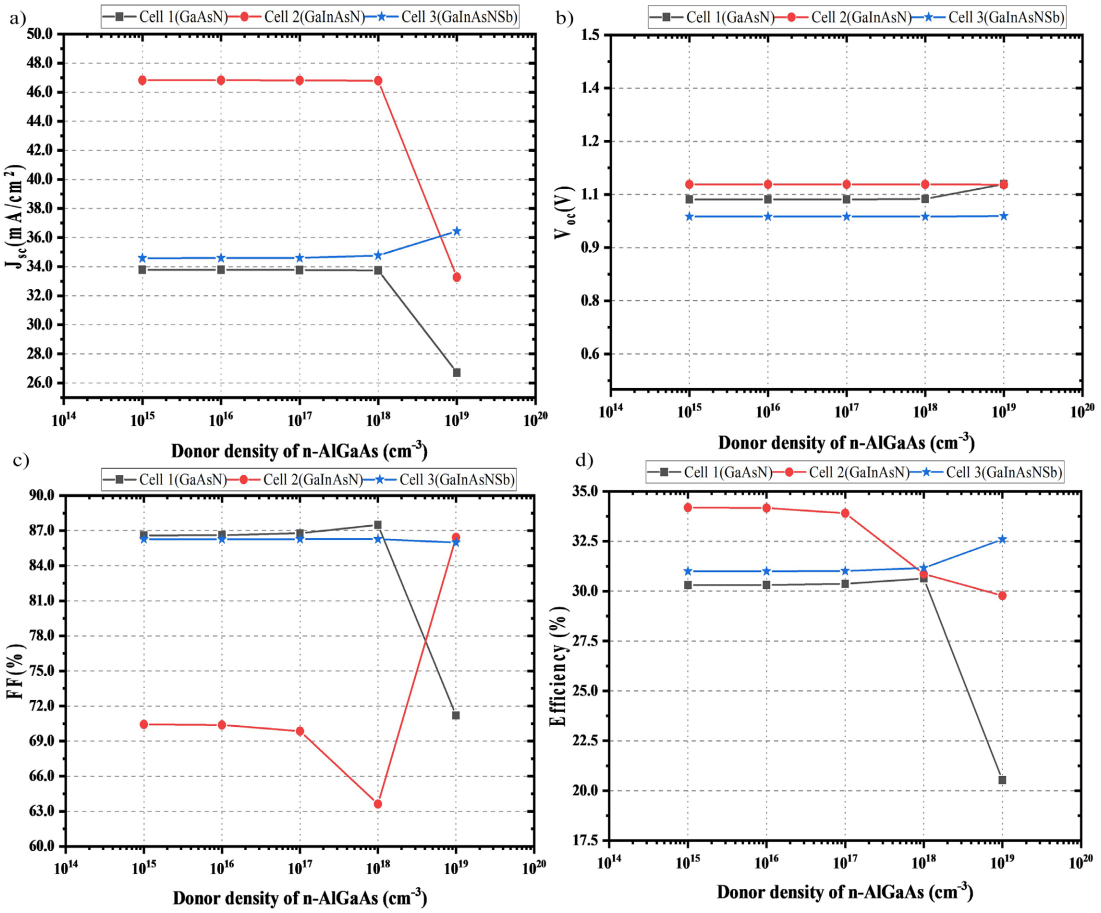

Figure 11. Impacts of n^- AlGaAs donor density on (a) J_{sc} (b) V_{oc} (c) FF (d) Efficiency, η on Photovoltaic (PV) solar cells.

3.11. Impact of Temperature on the Performance Parameters of the Solar Cells

Operating temperature has a vital impact on the solar cells performances [64]. In this section, the temperature was changed from 290 K to 325 K to take into account the influence of the working temperature on V_{oc}, J_{sc}, FF and η performances of dilute nitrides GaAsN, GaInAsN, and GaInAsNSb-based thin-film solar cells which have been illustrated in **Figure 12**.

As clarified in **Figure 12**, the performances of these three solar cell structures were greatly impacted by temperature changes. It is noticed for **Figure 12(b)** that as the temperature rises, V_{oc} drops distinctly for every material used in absorber layer. The reasons are that higher temperature shifts the band gap energy of the dilute nitrides to lower energy [65] and also simultaneously increases the velocity-instability of charged particles [66], reverse saturation current and resistivity of the materials as well. As a result, the probability of recombination rate of charge carriers before reaching the depletion region promotes and eventually degradation of V_{oc} occurs. Cell 1 (GaAsN) displays nearly stable J_{sc} and FF shown in **Fig-**

ure 12(a) and Figure 12(c) respectively but suffers a decline in V_{oc} and efficiency with increasing temperature as shown in Figure 12(d). The value of J_{sc} can be restricted by the device ohmic losses such as series and shunt resistances, metal contact and recombination losses. The constant current density with increasing temperature apparently indicates that the combined effects of these mentioned parameters might mitigate the variation in J_{sc} of GaAsN-based solar cell in our simulation. The behavior of the FF is possibly dependent on the combined behavior of V_{oc} and J_{sc} [62] [63]. Constant J_{sc} and decrement in V_{oc} jointly led to a decrease in FF of the device in Cell 1. Cell 2 (GaInAsN) exhibits nearly constant but large J_{sc} as well as efficiency with increasing temperature. Cell 3 (GaInAsNSb) gains the considerable rise in J_{sc} and efficiency with increasing temperature. The value of η reflects the total behavior of V_{oc}, J_{sc} and FF [67]. Increment in J_{sc} in large scale with small decrement in both V_{oc} and FF jointly leads the way to increase in the η of the Cell 3. Overall, although all three cells's V_{oc} drops with increased temperature, Cell 2 displays the largest overall performance, suggesting that GaInAsN is suitable for high-temperature settings, followed by GaInAsNSb, and GaAsN. In order to achieve better results, we also came to the conclusion that thin-film solar cells should be operated at 295 K.

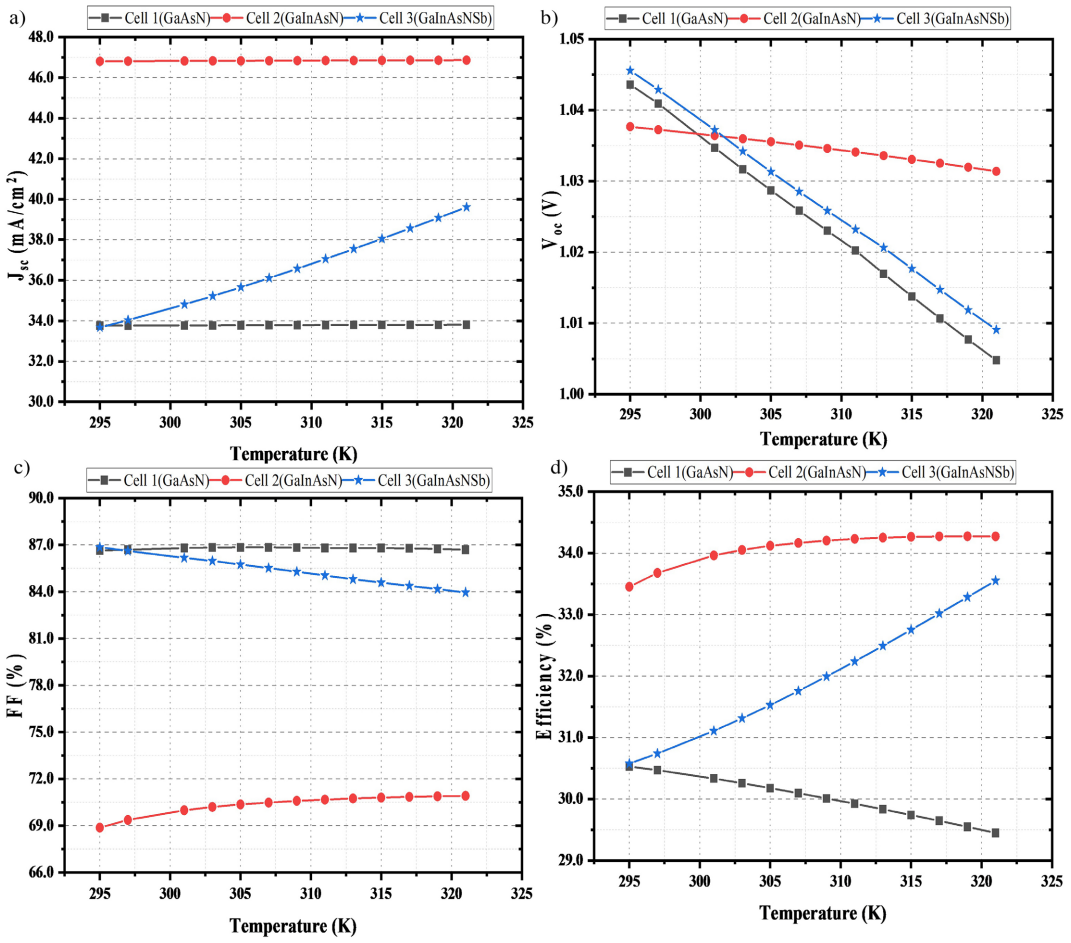

Figure 12. Effects of temperature on (a) J_{sc} (b) V_{oc} (c) FF (d) Efficiency, η in thin-film solar cells.

3.12. Quantum Efficiency (QE) of the Proposed Solar Cells

The quantum efficiency (QE) of the proposed GaAsN, GaInAsN, and GaInAsNSb-based thin-film solar cells structures as a function of wavelength has been demonstrated in Figure 13.

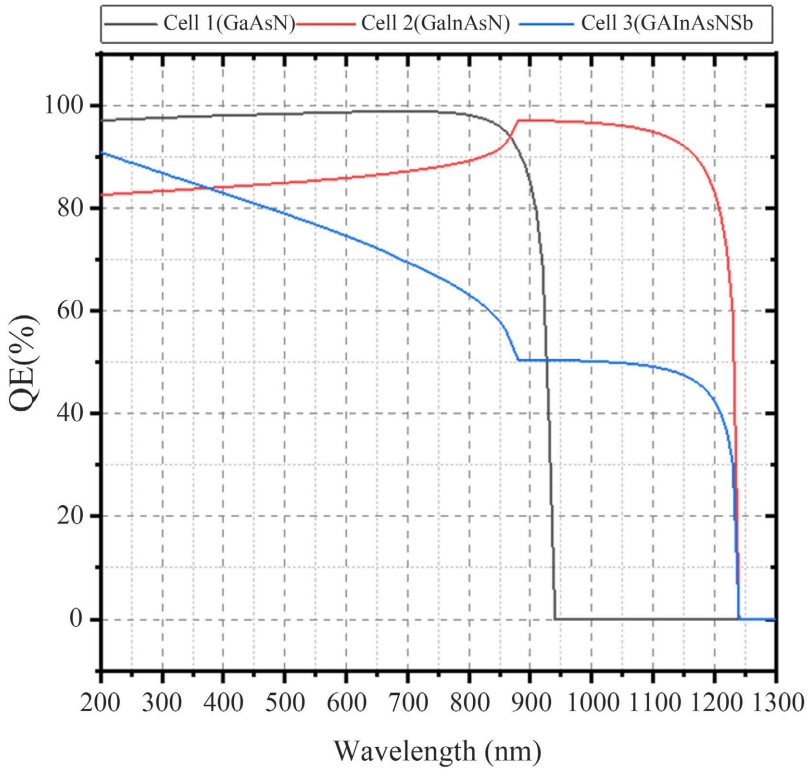

Figure 13. QE of the proposed solar cell structures as a function of wavelength.

It can be seen from that figure, Cell 1 (GaAsN) performs well in the visible and near-infrared regions (300 - 900 nm) of the incident light but abruptly loses efficiency in the infrared owing to its band-gap restrictions. On the other hand, Cell 2 (GaInAsN) beats Cell 1, with higher QE in the mid- to long-wavelength regions (400 - 1230 nm) notably in the near-infrared, due to the introduction of indium, which broadens the absorption spectrum. Cell 3 (GaInAsNSb) demonstrates the overall QE throughout a larger range, from 300 to 1230 nm, with the inclusion of both indium and antimony boosting absorption, lowering recombination, and prolonging photon capture. By making comparison among the three cells shown in Figure 13, it has been concluded that Cell 2 is the most effective at absorbing photons throughout both visible and infrared light, followed by Cell 3, whereas Cell 1 is confined to shorter wavelengths.

4. Conclusion

This study presents a comparative examination of thin-film solar cells containing GaAsN (Cell 1), GaInAsN (Cell 2), and GaInAsNSb (Cell 3) individually as absorber layer's material, modeled using SCAPS-1D. The data revealed that material

composition, absorber and other layer's thickness, doping densities, and ambient temperature greatly influence the photovoltaic performance metrics, such as J_{sc}, V_{oc}, FF, efficiency and QE. Among the three structures, Cell 2 (GaInAsN) resulted as the ideal choice, achieving the maximum efficiency (34.7%) and short-circuit current density (46.8 mA/cm^2). Cell 2 also demonstrated better quantum efficiency across the visible and near-infrared wavelengths, making it suited for high-performance photovoltaic applications. Additionally, it maintained robust performance throughout a wide range of absorber thicknesses, doping concentrations, and operating temperatures, proving its versatility and efficiency in varied settings. Cell 3 (GaInAsNSb) displayed an increased absorption range up to 1300 nm, owing to antimony inclusion, which improved carrier collection, reduced recombination losses, and enhanced stability. While its efficiency (31.6%) fell short of Cell 2, its steady performance under varied climatic and structural circumstances makes it a suitable contender for applications needing greater reliability. Cell 1 (GaAsN), while demonstrating acceptable performance metrics, was limited by its smaller absorption range and lower J_{sc} (33.8 mA/cm^2), resulting in a peak efficiency of 30.6%. This underlines the necessity for compositional adjustments, such as the incorporation of indium or antimony, to improve its performance. Overall, the work emphasizes the remarkable performance of GaInAsN for thin-film solar cells, combining high efficiency, excellent quantum efficiency, and adaptability. GaInAsNSb, with its increased stability and expanded absorption range, has promise for specialized applications. These findings would open the new door for further experimental study to optimize dilute nitride-based solar cells performance for next-generation photovoltaic technology.

Funding

The research works have been conducted by self-fund.

Data Availability Statement

The data of this study are available from the corresponding author upon reasonable request.

Acknowledgements

The authors would like to thank Marc Burgelman, Department of Electronics and Information System, University of Gent, Belgium for allowing the opportunity to use SCAPS-1D for simulation. They are also grateful to the Department of Electrical and Electronic Engineering, Hajee Mohammad Danesh Science and Technology University, Dinajpur-5200, Bangladesh for providing necessary technical supports.

Conflicts of Interest

According to the writers, they have no known conflicting financial interests or personal ties that may have an impact on the research presented in this article.

References

[1] Owusu, P.A. and Asumadu-Sarkodie, S. (2016) Sustainability Issues and Climate Change Mitigation: A Review of Renewable Energy Sources, Sustainability Issues and Climate Change Mitigation. *Cogent Engineering*, **3**, Article ID: 1167990. https://doi.org/10.1080/23311916.2016.1167990

[2] Ebhota, W.S. and Jen, T. (2019) Fossil Fuels Environmental Challenges and the Role of Solar Photovoltaic Technology Advances in Fast Tracking Hybrid Renewable Energy System. *International Journal of Precision Engineering and Manufacturing-Green Technology*, **7**, 97-117. https://doi.org/10.1007/s40684-019-00101-9

[3] Shiyani, T., Mahapatra, S.K. and Banerjee, I. (2023) Plasmonic Solar Cells. *Fundamentals of Solar Cell Design*, **16**, 55-81. https://doi.org/10.1002/9781119725022.ch2

[4] Bilgen, S. (2014) Structure and Environmental Impact of Global Energy Consumption. *Renewable and Sustainable Energy Reviews*, **38**, 890-902. https://doi.org/10.1016/j.rser.2014.07.004

[5] Islam, M.M. and Hasanuzzaman, M. (2020) Introduction to Energy and Sustainable Development. In: Hasanuzzaman, M.D. and Rahim, N.A., Eds., *Energy for Sustainable Development*, Elsevier, 1-18. https://doi.org/10.1016/b978-0-12-814645-3.00001-8

[6] Maka, A.O.M. and Alabid, J.M. (2022) Solar Energy Technology and Its Roles in Sustainable Development. *Clean Energy*, **6**, 476-483. https://doi.org/10.1093/ce/zkac023

[7] Kabir, E., Kumar, P., Kumar, S., Adelodun, A.A. and Kim, K. (2018) Solar Energy: Potential and Future Prospects. *Renewable and Sustainable Energy Reviews*, **82**, 894-900. https://doi.org/10.1016/j.rser.2017.09.094

[8] NREL (2021) Documenting a Decade of Cost Declines for PV Systems Documenting a Decade of Cost Declines for PV Systems. The National Renewable Energy Laboratory (NREL), 23-25. https://www.nrel.gov/news/program/2021/documenting-a-decade-of-cost-declines-for-pv-systems.html

[9] Li, F., Zhou, S., Yuan, J., Qin, C., Yang, Y., Shi, J., *et al.* (2019) Perovskite Quantum Dot Solar Cells with 15.6% Efficiency and Improved Stability Enabled by an α-$CsPbI_3$/$FAPbI_3$ Bilayer Structure. *ACS Energy Letters*, **4**, 2571-2578. https://doi.org/10.1021/acsenergylett.9b01920

[10] Yasodharan, R., Senthilkumar, A.P., Mohankumar, P., Ajayan, J. and Sivabalakrishnan, R. (2020) Investigation and Influence of Layer Composition of Tandem Perovskite Solar Cells for Applications in Future Renewable and Sustainable Energy. *Optik*, **212**, Article ID: 164723. https://doi.org/10.1016/j.ijleo.2020.164723

[11] Mazzucato, S., Royall, B., Ketlhwaafetse, R., Balkan, N., Salmi, J., Puustinen, J., *et al.* (2012) Dilute Nitride and GaAs N-I-P-I Solar Cells. *Nanoscale Research Letters*, **7**, Article No. 631. https://doi.org/10.1186/1556-276x-7-631

[12] Deshpande, R.A. (2021) Advances in Solar Cell Technology: An Overview. *Journal of Scientific Research*, **65**, 72-75. https://doi.org/10.37398/jsr.2021.650214

[13] Moon, S., Kim, K., Kim, Y., Heo, J. and Lee, J. (2016) Highly Efficient Single-Junction Gaas Thin-Film Solar Cell on Flexible Substrate. *Scientific Reports*, **6**, Article No. 30107. https://doi.org/10.1038/srep30107

[14] Elshorbagy, M.H., Abdel-Hady, K., Kamal, H. and Alda, J. (2017) Broadband Anti-Reflection Coating Using Dielectric Si3n4 Nanostructures. Application to Amorphous-Si-H Solar Cells. *Optics Communications*, **390**, 130-136. https://doi.org/10.1016/j.optcom.2016.12.062

[15] Chopra, K.L., Paulson, P.D. and Dutta, V. (2004) Thin-Film Solar Cells: An Overview. *Progress in Photovoltaics*: *Research and Applications*, **12**, 69-92. https://doi.org/10.1002/pip.541

[16] Bi, W.G. and Tu, C.W. (1997) Bowing Parameter of the Band-Gap Energy of GaN_xAs_{1-x}. *Applied Physics Letters*, **70**, 1608-1610. https://doi.org/10.1063/1.118630

[17] Miyoshi, S., Yaguchi, H., Onabe, K., Ito, R. and Shiraki, Y. (1993) Metalorganic Vapor Phase Epitaxy of $GaP_{1-x}N_x$ alloys on GaP. *Applied Physics Letters*, **63**, 3506-3508. https://doi.org/10.1063/1.110109

[18] Bellaiche, L., Wei, S. and Zunger, A. (1997) Band Gaps of GaPN and GaAsN Alloys. *Applied Physics Letters*, **70**, 3558-3560. https://doi.org/10.1063/1.119232

[19] Bi, W.G. and Tu, C.W. (1996) N Incorporation in InP and Band Gap Bowing of InN_xP_{1-x}. *Journal of Applied Physics*, **80**, 1934-1936. https://doi.org/10.1063/1.362945

[20] Weyers, M., Michio Sato, M.S. and Hiroaki Ando, H.A. (1992) Red Shift of Photoluminescence and Absorption in Dilute GaAsN Alloy Layers. *Japanese Journal of Applied Physics*, **31**, L853. https://doi.org/10.1143/jjap.31.l853

[21] Luque, A. and Martí, A. (1997) Increasing the Efficiency of Ideal Solar Cells by Photon Induced Transitions at Intermediate Levels. *Physical Review Letters*, **78**, 5014-5017. https://doi.org/10.1103/physrevlett.78.5014

[22] Haque, M.D., Ali, M.H., Hossain, M.M., Hossain, M.S., Hossain, M.I., Halim, M.A., *et al.* (2022) Design and Analysis of GaAsN Based Solar Cell for Harvesting Visible to Near-Infrared Light. *Physica Scripta*, **97**, Article ID: 085006. https://doi.org/10.1088/1402-4896/ac7d79

[23] Wang, L., Elleuch, O., Kojima, N., Ohshita, Y. and Yamaguchi, M. (2014) Simulation Analysis of the Potential Causes for the Low Jsc in GaAsN Solar Cells. *Extended Abstracts of the* 2014 *International Conference on Solid State Devices and Materials*, Ibaraki, 8-11 September 2014, 390-400. https://doi.org/10.7567/ssdm.2014.ps-15-1

[24] Krispin, P., Gambin, V., Harris, J.S. and Ploog, K.H. (2003) Nitrogen-Related Electron Traps in Ga (As, N) Layers ($\leq$ 3% N). *Journal of Applied Physics*, **93**, 6095-6099. https://doi.org/10.1063/1.1568523

[25] Yaguchi, H., Morioke, T., Aoki, T., Hijikata, Y., Yoshida, S., Akiyama, H., *et al.* (2003) Improvement in the Luminescence Efficiency of GaAsN Alloys by Photoexcitation. *Physica Status Solidi* (*c*), **0**, 2782-2784. https://doi.org/10.1002/pssc.200303514

[26] Kondow, M., Uomi, K., Niwa, A., Kitatani, T., Watahiki, S. and Yazawa, Y. (1996) GaInNAs: A Novel Material for Long-Wavelength-Range Laser Diodes with Excellent High-Temperature Performance. *Japanese Journal of Applied Physics*, **35**, Article 1273. https://doi.org/10.1143/jjap.35.1273

[27] Sabnis, V., Yuen, H. and Wiemer, M. (2012) High-Efficiency Multijunction Solar Cells Employing Dilute Nitrides. *AIP Conference Proceedings*, **1477**, 14-19. https://doi.org/10.1063/1.4753823

[28] Friedman, D.J., Geisz, J.F., Kurtz, S.R. and Olson, J.M. (1998) 1-eV Solar Cells with Gainnas Active Layer. *Journal of Crystal Growth*, **195**, 409-415. https://doi.org/10.1016/s0022-0248(98)00561-2

[29] Kurtz, S.R., Allerman, A.A., Jones, E.D., Gee, J.M., Banas, J.J. and Hammons, B.E. (1999) InGaAsN Solar Cells with 1.0 Ev Band Gap, Lattice Matched to Gaas. *Applied Physics Letters*, **74**, 729-731. https://doi.org/10.1063/1.123105

[30] Jackrel, D.B., Bank, S.R., Yuen, H.B., Wistey, M.A., Harris, J.S., Ptak, A.J., *et al.* (2007) Dilute Nitride GaInNAs and GaInNAsSb Solar Cells by Molecular Beam Epitaxy.

Journal of Applied Physics, **101**, Article ID: 114916.
https://doi.org/10.1063/1.2744490

[31] Kondow, M., Kitatani, T., Nakatsuka, S., Larson, M.C., Nakahara, K., Yazawa, Y., *et al.* (1997) GaInNAs: A Novel Material for Long-Wavelength Semiconductor Lasers. *IEEE Journal of Selected Topics in Quantum Electronics*, **3**, 719-730. https://doi.org/10.1109/2944.640627

[32] Kitatani, T., Nakahara, K., Kondow, M., Uomi, K. and Tanaka, T. (2000) A 1.3-μm GaInNAs/GaAs Single-Quantum-Well Laser Diode with a High Characteristic Temperature over 200 K. *Japanese Journal of Applied Physics*, **39**, L86. https://doi.org/10.1143/jjap.39.l86

[33] Sato, S. (2000) Low Threshold and High Characteristic Temperature 1.3 μm Range GaInNAs Lasers Grown by Metalorganic Chemical Vapor Deposition. *Japanese Journal of Applied Physics*, **39**, Article 3403. https://doi.org/10.1143/jjap.39.3403

[34] Riechert, H., Egorov, A.Y., Livshits, D., Borchert, B. and Illek, S. (2000) InGaAsN/GaAs Heterostructures for Long-Wavelength Light-Emitting Devices. *Nanotechnology*, **11**, 201-205. https://doi.org/10.1088/0957-4484/11/4/301

[35] Fischer, M., Gollub, D. and Forchel, A. (2002) 1.3 μm GaInAsN Laserdiodes with Improved High Temperature Performance. *Japanese Journal of Applied Physics*, **41**, 1162-1163. https://doi.org/10.1143/jjap.41.1162

[36] Lin, Y., Ma, T., Chen, T. and Lin, H. (2008) Energy Gap Reduction in Dilute Nitride GaAsSbN. *Applied Physics Letters*, **93**, Article ID: 171914. https://doi.org/10.1063/1.3009199

[37] Isoaho, R., Aho, A., Tukiainen, A., Salminen, T. and Guina, M. (2022) Bandgap Energy Model for GaInNAsSb/GaAs Alloys with High N Content and Strain Influence. *Journal of Crystal Growth*, **584**, Article ID: 126574. https://doi.org/10.1016/j.jcrysgro.2022.126574

[38] Harris, J.S., Kudrawiec, R., Yuen, H.B., Bank, S.R., Bae, H.P., Wistey, M.A., *et al.* (2007) Development of GaInNAsSb Alloys: Growth, Band Structure, Optical Properties and Applications. *Physica Status Solidi* (*b*), **244**, 2707-2729. https://doi.org/10.1002/pssb.200675620

[39] Yang, X., Jurkovic, M.J., Heroux, J.B. and Wang, W.I. (1999) Molecular Beam Epitaxial Growth of InGaAsN:Sb/GaAs Quantum Wells for Long-Wavelength Semiconductor Lasers. *Applied Physics Letters*, **75**, 178-180. https://doi.org/10.1063/1.124311

[40] Isoaho, R., Aho, A., Tukiainen, A., Aho, T., Raappana, M., Salminen, T., *et al.* (2019) Photovoltaic Properties of Low-Bandgap (0.7-0.9 eV) Lattice-Matched GaInNAsSb Solar Junctions Grown by Molecular Beam Epitaxy on GaAs. *Solar Energy Materials and Solar Cells*, **195**, 198-203. https://doi.org/10.1016/j.solmat.2019.02.030

[41] Lin, Q., Huang, H., Jing, Y., Fu, H., Chang, P., Li, D., *et al.* (2014) Flexible Photovoltaic Technologies. *Journal of Materials Chemistry C*, **2**, 1233-1247. https://doi.org/10.1039/c3tc32197e

[42] Galiana, B., Rey-Stolle, I., Baudrit, M., García, I. and Algora, C. (2006) A Comparative Study of BSF Layers for GaAs-Based Single-Junction or Multijunction Concentrator Solar Cells. *Semiconductor Science and Technology*, **21**, 1387-1392. https://doi.org/10.1088/0268-1242/21/10/003

[43] Wagle, R., Gaib, R., Shrivastava, A. and Nath Mishra, L. (2020) Modelling and Simulation of AlGaAs/GaAs Solar Cell. *American journal of Engineering Research*, **9**, 218-223. https://www.ajer.org

[44] Holman, Z.C., De Wolf, S. and Ballif, C. (2013) Improving Metal Reflectors by Suppressing Surface Plasmon Polaritons: A Priori Calculation of the Internal Reflectance of a Solar Cell. *Light*: *Science & Applications*, **2**, e106. https://doi.org/10.1038/lsa.2013.62

[45] Baker-Finch, S.C. and McIntosh, K.R. (2010) Reflection of Normally Incident Light from Silicon Solar Cells with Pyramidal Texture. *Progress in Photovoltaics*: *Research and Applications*, **19**, 406-416. https://doi.org/10.1002/pip.1050

[46] Narayanamurti, V., Kozhevnikov, M., Xin, H.P., Tu, C.W., Mascarenhas, A. and Zhang, Y. (2000) Nitrogen-Induced Evolution of GaAs1-xNx Studied by Ballistic Electron Emission Spectroscopy. *NCPV Program Review Metting*, *National Renewable Energy Lab* (NREL), Colorado, 16-19 April 2000, 7-8.

[47] Milanova, M., Vitanov, P., Terziyska, P., Koleva, G. and Popov, G. (2013) Nitrogen Incorporation into GaAsN and InGaAsN Layers Grown by Liquid-Phase Epitaxy. *Physica Status Solidi C*, **10**, 597-600. https://doi.org/10.1002/pssc.201200890

[48] Yuen, H.B., Bank, S.R., Bae, H., Wistey, M.A. and Harris, J.S. (2006) The Role of Antimony on Properties of Widely Varying GaInNAsSb Compositions. *Journal of Applied Physics*, **99**, Article ID: 093504. https://doi.org/10.1063/1.2191745

[49] Verschraegen, J. and Burgelman, M. (2007) Numerical Modeling of Intra-Band Tunneling for Heterojunction Solar Cells in SCAPS. *Thin Solid Films*, **515**, 6276-6279. https://doi.org/10.1016/j.tsf.2006.12.049

[50] Hima, A. and Lakhdar, N. (2020) Enhancement of Efficiency and Stability of $CH_3NH_3GeI_3$ solar cells with $CuSbS_2$. *Optical Materials*, **99**, Article ID: 109607. https://doi.org/10.1016/j.optmat.2019.109607

[51] Pindolia, G., Shinde, S.M. and Jha, P.K. (2022) Optimization of an Inorganic Lead Free $RbGeI_3$ Based Perovskite Solar Cell by SCAPS-1D Simulation. *Solar Energy*, **236**, 802-821. https://doi.org/10.1016/j.solener.2022.03.053

[52] Boumesjed, A., Mazari, H. and Ameur, K. (2018) Predicted Theoretical Efficiency for New Intermediate Band Solar Cells (IBSC) Based on $GaAs_{1-x}N_x$. *Journal of New Technology and Materials*, **8**, 102-109. https://doi.org/10.12816/0048938

[53] Tang, D., Vijaya, G.K., Mehrotra, A., Freundlich, A. and Smith, D.J. (2016) Investigation of Dilute-Nitride Alloys of $GaAsN_x$ ($0.01 < X < 0.04$) Grown by MBE on Gaas (001) Substrates for Photovoltaic Solar Cell Devices. *Journal of Vacuum Science & Technology B*, *Nanotechnology and Microelectronics*: *Materials*, *Processing*, *Measurement*, *and Phenomena*, **34**, Article ID: 011210. https://doi.org/10.1116/1.4940127

[54] Tukiainen, A., Aho, A., Polojarvi, V., Ahorinta, R. and Guina, M. (2016) High Efficiency Dilute Nitride Solar Cells: Simulations Meet Experiments. *Journal of Green Engineering*, **5**, 113-132. https://doi.org/10.13052/jge1904-4720.5348

[55] Loke, W.K., Yoon, S.F., Wicaksono, S., Tan, K.H. and Lew, K.L. (2007) Defect-induced Trap-Assisted Tunneling Current in GaInNAs Grown on Gaas Substrate. *Journal of Applied Physics*, **102**, Article ID: 054501. https://doi.org/10.1063/1.2775908

[56] Volz, K., Stolz, W., Teubert, J., Klar, P.J., Heimbrodt, W., Dimroth, F., *et al.* (n.d.) Doping, Electrical Properties and Solar Cell Application of GaInNAs. In: Erol, A., Ed., *Dilute III- V Nitride Semiconductors and Material Systems*, Springer, 369-404. https://doi.org/10.1007/978-3-540-74529-7_15

[57] Li, S., Soong, W.M., Steer, M.J., Zhang, S. and Ng, J.S. (2012) Dilute Nitride GaInNAs and GaInNAsSb for Solar Cell Application. *SPIE OPTO-Physics*, *Simulation*, *and Photonic Engineering of Photovoltaic Devices*, California, 21 February 2012, 82561E:34.

[58] Hwang, S., Kim, S., Cheun, H., Lee, H., Lee, B., Hwang, T., *et al.* (2016) Bandgap

Grading and $Al_{0.3}Ga_{0.7}As$ Heterojunction Emitter for Highly Efficient GaAs-Based Solar Cells. *Solar Energy Materials and Solar Cells*, **155**, 264-272. https://doi.org/10.1016/j.solmat.2016.06.009

[59] Chan, H. and Shieh, T. (1991) A Three Dimensional Semiconductor Device Simulator for GaAs/AlGaAs Heterojunction Bipolar Transistor Analysis. *IEEE Transactions on Electron Devices*, **38**, 2427-2432. https://doi.org/10.1109/16.97405

[60] Debbar, N. and Al-Mashary, B. (2003) Numerical Simulation of GaAs/AlGaAs Heterojunctions Including Interface States and Thermionic Emission. *International Journal of Modelling and Simulation*, **23**, 103-108. https://doi.org/10.1080/02286203.2003.11442260

[61] Ouslimane, T., Et-taya, L., Elmaimouni, L. and Benami, A. (2021) Impact of Absorber Layer Thickness, Defect Density, and Operating Temperature on the Performance of $MAPbI_3$ Solar Cells Based on ZnO Electron Transporting Material. *Heliyon*, **7**, e06379. https://doi.org/10.1016/j.heliyon.2021.e06379

[62] Singh, P. and Ravindra, N.M. (2012) Temperature Dependence of Solar Cell Performance—An Analysis. *Solar Energy Materials and Solar Cells*, **101**, 36-45. https://doi.org/10.1016/j.solmat.2012.02.019

[63] Abdelfatah, M., Ledig, J., El-Shaer, A., Wagner, A., Marin-Borras, V., Sharafeev, A., *et al.* (2016) Fabrication and Characterization of Low Cost Cu_2O/ZnO:Al Solar Cells for Sustainable Photovoltaics with Earth Abundant Materials. *Solar Energy Materials and Solar Cells*, **145**, 454-461. https://doi.org/10.1016/j.solmat.2015.11.015

[64] Daoudia, A.K., El Hassouani, Y. and Benami, A. (2016) Investigation of the Effect of Thickness, Band Gap and Temperature on the Efficiency of CIGS Solar Cells through SCAPS-1D. *International Journal of Engineering Research & Technology*, **6**, 71.

[65] Varshni, Y.P. (1967) Temperature Dependence of the Energy Gap in Semiconductors. *Physica*, **34**, 149-154. https://doi.org/10.1016/0031-8914(67)90062-6

[66] Alam, I. and Ashraf, M.A. (2020) Effect of Different Device Parameters on Tin-Based Perovskite Solar Cell Coupled with In_2S_3 Electron Transport Layer and CuSCN and Spiro-OMeTAD Alternative Hole Transport Layers for High-Efficiency Performance. *Energy Sources, Part A: Recovery, Utilization, and Environmental Effects*, **46**, 17080-17096. https://doi.org/10.1080/15567036.2020.1820628

[67] Baloch, A.A.B., Aly, S.P., Hossain, M.I., El-Mellouhi, F., Tabet, N. and Alharbi, F.H. (2017) Full Space Device Optimization for Solar Cells. *Scientific Reports*, **7**, Article No. 11984. https://doi.org/10.1038/s41598-017-12158-0